National Technical Information Service
Accession Report No. AD-

JRC-74-99

SEISMOACOUSTIC WAVES IN WATER-COVERED SAND

Jacques R. Chamuel
December 1999

Sonoquest Advanced Ultrasonics Research
P. O. Box 81153, Wellesley Hills, Massachusetts 02481-0001, USA

This report is available from National Technical Information Service, U. S. Dept. of Commerce, 5285 Port Royal Road, Springfield, VA 22161 Tel. (703) 487-4650

REPORT DOCUMENTATION PAGE

Form Approved
OMB No. 0704-0188

1. AGENCY USE ONLY (Leave blank)	2. REPORT DATE	3. REPORT TYPE AND DATES COVERED
	December 1999	Final Report May 97 - Dec 99

4. TITLE AND SUBTITLE

SEISMOACOUSTIC WAVES IN WATER-COVERED SAND

5. FUNDING NUMBERS

C -
N00014-97-C-0065

6. AUTHOR(S)

Jacques R. Chamuel

7. PERFORMING ORGANIZATION NAME(S) AND ADDRESS(ES)

Sonoquest Advanced Ultrasonics Research
P. O. Box 81153
Wellesley Hills, MA 02481-0001

8. PERFORMING ORGANIZATION REPORT NUMBER

JRC-74-99

9. SPONSORING/MONITORING AGENCY NAME(S) AND ADDRESS(ES)

Office of Naval Research

10. SPONSORING/MONITORING AGENCY REPORT NUMBER

11. SUPPLEMENTARY NOTES

ONR POC - Dr. Jeffrey Simmen (703) 696-4204

12a. DISTRIBUTION/AVAILABILITY STATEMENT

Approved for Public Release

12b. DISTRIBUTION CODE

13. ABSTRACT *(Maximum 200 words)*

A collection of new findings are presented contributing to fundamental physical understanding of broadband (3-500 KHz) transient seismoacoustic wave phenomena in various sand conditions (water-saturated, naturally settled, disturbed, drained, liquefied, compacted, water-covered, air bubbles) important for acoustic modeling of seafloor and predicting the penetration and conversion of seismoacaoustic waves in sediments. The experimental results compare waveforms of different types of seismoacoustic waves. An explanation is given for the anomalous slow compressional wave observed in water-saturated sand by Boyle and Chotiros (1992). Other experimental results presented include a) the effect of ripples on surface and interface waves dispersion, b) the existence of high-frequency fast compressional waves (1650 m/s) in drained sand, c) the effect of puddles and water edges on converting interface waves into body shear waves, f) the nonexistence of a second Rayleigh wave along with Scholte wave in soft sediments, and g) the first experimental results on wedge waves along the edge of sand dollar skeletons.

14. SUBJECT TERMS

underwater acoustics, sand, ripples, slow wave, Scholte wave, seismoacoustic, bubbles, compressional, Rayleigh,sediments

15. NUMBER OF PAGES

43

16. PRICE CODE

17. SECURITY CLASSIFICATION OF REPORT	18. SECURITY CLASSIFICATION OF THIS PAGE	19. SECURITY CLASSIFICATION OF ABSTRACT	20. LIMITATION OF ABSTRACT
Unclassified	Unclassified	Unclassified	UL

GENERAL INSTRUCTIONS FOR COMPLETING SF 298

The Report Documentation Page (RDP) is used in announcing and cataloging reports. It is important that this information be consistent with the rest of the report, particularly the cover and title page. Instructions for filling in each block of the form follow. It is important to ***stay within the lines*** to meet ***optical scanning requirements***.

Block 1. Agency Use Only *(Leave blank)*.

Block 2. Report Date. Full publication date including day, month, and year, if available (e.g. 1 Jan 88). Must cite at least the year.

Block 3. Type of Report and Dates Covered. State whether report is interim, final, etc. If applicable, enter inclusive report dates (e.g. 10 Jun 87 - 30 Jun 88).

Block 4. Title and Subtitle. A title is taken from the part of the report that provides the most meaningful and complete information. When a report is prepared in more than one volume, repeat the primary title, add volume number, and include subtitle for the specific volume. On classified documents enter the title classification in parentheses.

Block 5. Funding Numbers. To include contract and grant numbers; may include program element number(s), project number(s), task number(s), and work unit number(s). Use the following labels:

C	- Contract	**PR**	- Project
G	- Grant	**TA**	- Task
PE	- Program Element	**WU**	- Work Unit Accession No.

Block 6. Author(s). Name(s) of person(s) responsible for writing the report, performing the research, or credited with the content of the report. If editor or compiler, this should follow the name(s).

Block 7. Performing Organization Name(s) and Address(es). Self-explanatory.

Block 8. Performing Organization Report Number. Enter the unique alphanumeric report number(s) assigned by the organization performing the report.

Block 9. Sponsoring/Monitoring Agency Name(s) and Address(es). Self-explanatory.

Block 10. Sponsoring/Monitoring Agency Report Number. *(If known)*

Block 11. Supplementary Notes. Enter information not included elsewhere such as: Prepared in cooperation with...; Trans. of...; To be published in.... When a report is revised, include a statement whether the new report supersedes or supplements the older report.

Block 12a. Distribution/Availability Statement. Denotes public availability or limitations. Cite any availability to the public. Enter additional limitations or special markings in all capitals (e.g. NOFORN, REL, ITAR).

DOD	- See DoDD 5230.24, "Distribution Statements on Technical Documents."
DOE	- See authorities.
NASA	- See Handbook NHB 2200.2.
NTIS	- Leave blank.

Block 12b. Distribution Code.

DOD	- Leave blank.
DOE	- Enter DOE distribution categories from the Standard Distribution for Unclassified Scientific and Technical Reports.
NASA	- Leave blank.
NTIS	- Leave blank.

Block 13. Abstract. Include a brief *(Maximum 200 words)* factual summary of the most significant information contained in the report.

Block 14. Subject Terms. Keywords or phrases identifying major subjects in the report.

Block 15. Number of Pages. Enter the total number of pages.

Block 16. Price Code. Enter appropriate price code *(NTIS only)*.

Blocks 17. - 19. Security Classifications. Self-explanatory. Enter U.S. Security Classification in accordance with U.S. Security Regulations (i.e., UNCLASSIFIED). If form contains classified information, stamp classification on the top and bottom of the page.

Block 20. Limitation of Abstract. This block must be completed to assign a limitation to the abstract. Enter either UL (unlimited) or SAR (same as report). An entry in this block is necessary if the abstract is to be limited. If blank, the abstract is assumed to be unlimited.

ABSTRACT

A collection of new findings are presented contributing to fundamental physical understanding of broadband (3-300 KHz) transient seismoacoustic wave phenomena in various sand conditions (water-saturated, naturally deposited, disturbed, drained, liquefied, compacted, and water-covered) important for acoustic modeling of seafloor and predicting the penetration and conversion of seismoacaoustic waves in sediments The experimental results compare waveforms of different types of seismoacoustic waves. An explanation is given for the anomalous slow compressional wave observed in water-saturated sand by Boyle and Chotiros (1992). Other experimental results presented include a) the effect of ripples on surface and interface waves dispersion, b) the existence of high-frequency fast compressional waves (1650 m/s) in drained sand, c) the effect of puddles, water edges, and liquefied regions on converting interface waves into body shear waves, f) the nonexistence of a second Rayleigh wave along with Scholte wave in soft sediments, and g) the first experimental results on wedge waves along the edge of sand dollar skeletons.

ACKNOWLEDGEMENTS

The research presented in this report was sponsored by the U.S. Office of Naval Research (ONR) Code 321OA under Contract No. N00014-97-C-0065. The author is indebted to Dr. Jeffrey Simmen / ONR for making this research possible.

TABLE OF CONTENTS

SUMMARY

Little is known about the seismoacoustic properties of water-saturated and partially saturated sandy marine sediments in the frequency range 1-100 KHz. Sand is an unstable medium and can change from a liquefied state to a varying stiff matrix depending on vibration, water content, pressure, air bubbles, and aging. In the surf zone, the acoustic conditions are complicated because of several factors (water dynamics, air bubbles in sediments and water, sand ripples, sea shells, buried shell fragments, tides, density and velocity gradients, sand dollar beds, sorted particles, settling of transported sediments, puddles and water edges, and biological activities) as depicted in Fig.1.

It is essential to study the fundamental seismoacoustic properties of water-saturated and partially saturated sand under controlled laboratory settings to determine the different types of seismoacoustic waves existing under various sand conditions, and validate current theoretical models. A number of unresolved controversial problems have been reported on the 60 KHz anomalous slow compressional wave (1200 m/s) observed by Boyle and Chotiros [1] in water-saturated sand, and the acoustic penetration of sandy sediments at incidence angles greater than Snell's critical angles [1-2]. The problem is complex because a) the shear wave velocity in water-saturated sand increases rapidly with depth as shown in Fig. 2 indicating that penetrating acoustic waves would experience strong upward refraction and conversion, b) at 60 KHz, the shear wavelength is about 5 grains of sand, and the validity of theoretical transmission coefficient calculations are questionable when the grain dimension is comparable to the wavelength, and c) the seismoacoustic properties of sandy sediments are not understood in the frequency range 3-80 KHz. Another current controversial fundamental problem is the physical interpretation of the

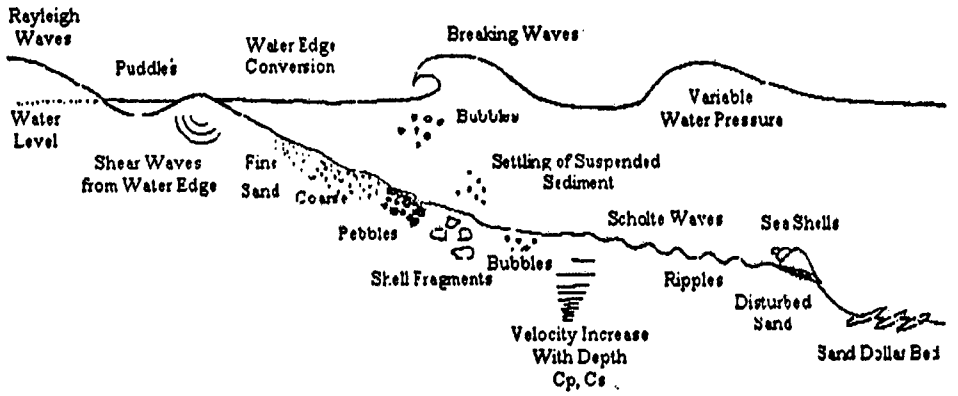

Fig. 1. Diagram depicting examples of factors affecting seismoacoustic properties of sandy seafloor in the surf zone.

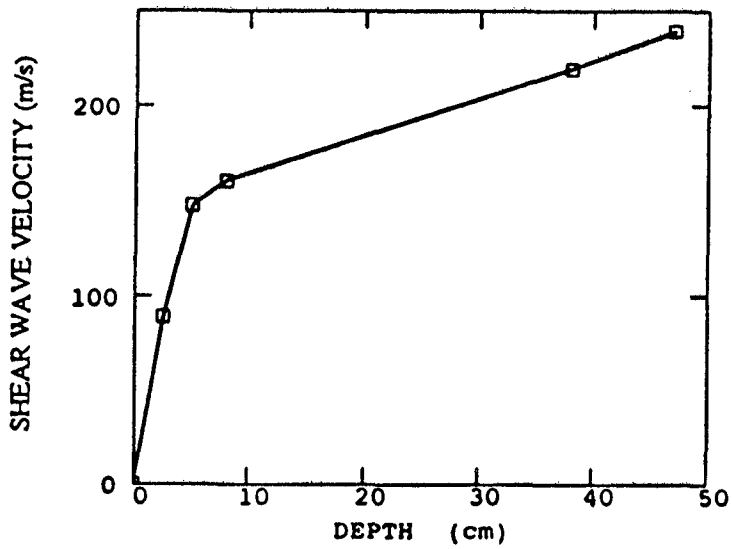

Fig. 2. Measured shear wave velocity at different depth in water-saturated sand using a broadband pulse with 35 KHz center frequency.

roots of the dispersion equation corresponding to the Rayleigh and Scholte waves [3-4] at a fluid-solid interface when the fluid velocity is between the shear wave velocity and the compressional wave velocity in the solid (e.g. sandy sediments, Plexiglas). Only a Scholte wave is known to exist at such interface, however, Padilla et al. [3] reported theoretical and experimental results apparently indicating the coexistence of a Rayleigh wave and a Scholte wave at a water/Plexiglas interface. Several new seismoacoustic findings were obtained while investigating the controversial problems mentioned above. The goal of the research was to develop better fundamental physical understanding of seismoacoustic phenomena in sandy sediments. The efforts were focused on identifying gaps in current understanding and suggest future quantitative research needed for accurate modeling of seafloor and seismoacoustic detection of buried objects.

The new findings are summarized in five different sections. **SECTION 1** provides an explanation [5] for the time of arrival of the anomalous slow compressional wave [1] based on the depth-dependence of the shear wave velocity. Several hypotheses were reported in the literature as summarized in [5-13]. Roughness along the water/sand interface can convert near-grazing acoustic waves into seismoacoustic waves in the sediment [11, 14-15]. The scattered field from roughness propagates laterally in the sediment with the fast compressional wave velocity ~1700 m/s and consists of multiple delayed components spread over a wide time window. The propagation time of a distinct 1200 m/s wave could not be explained from randomly distributed roughness. Fig. 3 demonstrates the effect of a periodic interface roughness on generating multiple delayed fast compressional waves using a laboratory water/Plexiglas ultrasonic model. The presence of surface roughness also introduces dispersion of interface waves. **SECTION 2** shows the effect of ripples on the dispersion of Rayleigh and Scholte waves. The results revealed that a corrugated surface can decrease the velocity of Rayleigh and Scholte waves by more than 70% [16].

In **SECTION 3**, waveforms from various sand conditions (water-saturated, naturally deposited, disturbed, drained, liquefied, compacted, and water-covered) are compared. Two surprising results were obtained. The first was that the measured velocity of high-frequency (100 KHz) compressional waves in naturally settled water-saturated sand remained near 1700 m/s when the sand was drained and did not drop to ~200 m/s as anticipated from the results of Velea [17], and Tavossi and Tittman [18] near 10 KHz. The decrease in density as air bubbles replaced the water in drained sand may have been counteracted by an increase in stiffness of the matrix due to capillary forces. Further quantitative research in needed. The second surprising result was the coexistence of a broadband fast compressional wave and a slow dispersive low-frequency compressional wave in water-covered disturbed sand with trapped air bubbles. It is not yet understood whether a dispersive Biot wave is superimposed over this slow compressional wave in coarse sand. **SECTION 4** shows the effect of water edge and puddles on converting interface waves into shear waves. Other experimental results demonstrate the existence of only one Scholte wave at a water/Plexiglas interface contradicting the results of Padilla et al. [3], and provided an explanation for the excessive amplitude decay of the apparent "Rayleigh" wave component described in [3]. **SECTION 5** presents the first experimental results on nondispersive flexural wedge waves along the edge of sand dollar skeletons that may play a role in underwater acoustic interaction with a seafloor covered with a single-age group sand dollar bed. In the **CONCLUSION**, several unanswered questions are presented suggesting needed future quantitative research leading to reliable detection of buried objects.

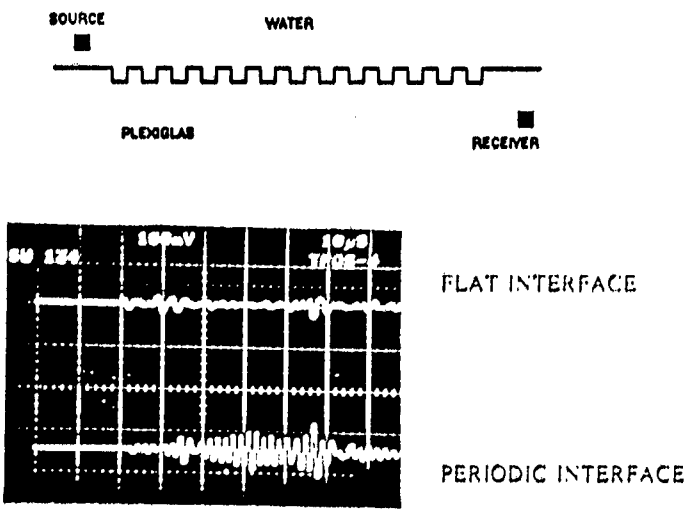

Fig. 3. Effect of periodic roughness on converting near-grazing underwater acoustic waves into laterally propagating compressional waves in elastic bottom. **Top**: Received waveform from flat interface. **Bottom**: Waveform from periodic interface. (Water/Plexiglas model with spatial wavelength 6.34 cm and groove depth 3 mm, compressional velocity = 2701 m/s, range = 15 cm, horizontal time scale 10 μs/div., time at beginning of trace 40 μs).

SECTION 1

Anomalous Slow Compressional Wave And Acoustic Penetration

1.1 An Explanation for the Anomalous Slow Wave in Water-Saturated Sand

Letters

An Explanation for the Anomalous Ultrasonic Slow Wave in Underwater Sand

Jacques R. Chamuel, *Member, IEEE*

***Abstract*—An explanation is given for the propagation time of the well-known anomalous ultrasonic slow wave observed in water-saturated sand using a three-layer elastic model. The rapid increase of elastic properties of sand with depth causes conversion of near-grazing underwater acoustic waves into multiple coupled shear and compressional waves.**

I. Introduction

Laboratory experimental studies by Muir *et al.* [1] on the transmission of near-grazing underwater ultrasonic waves into a smooth sandy bottom revealed that unexplained acoustic wave penetration occurred at angles of incidence greater than the critical angle. Chotiros [2], Boyle and Chotiros [3], and Altenburg and Chotiros [4] observed an anomalous ultrasonic wave in water-saturated sand that seemed to propagate with a velocity near 1200 m/s at 60 KHz. Chotiros [2] suggested that the anomalous wave was the slow compressional wave in porous media predicted by Biot [5], and proposed new poroelastic parameter values because, according to Biot's theory, the slow wave in water-saturated sand should be highly attenuated and should have a velocity about three times slower than this anomalous wave. Stoll [7] commented on inconsistencies related to the input parameters to the Biot theory chosen by Chotiros [2]. The Biot slow wave was not conclusively detected in water-saturated sand [8].

Substantial research was conducted on the anomalous slow acoustic wave and on the poroelastic properties of unconsolidated sand [2]–[4], [6]–[14] (partial list). Researchers came up with different hypotheses as summarized by Maguer *et al.* [10]. The four possible explanations given were: poroelastic Biot's theory and its associated second slow wave, water/sediment interface roughness [11], narrow beam effects [9], and evanescent wave scattering by volume inhomogeneities [12]. In addition, Yamamoto *et al.* [13] reported that disturbances in the seabed for instrumentation act as vertical waveguides that can be mistaken as a false Biot slow wave. The aim of this letter is to propose a layered elastic model as a hypothesis to explain the travel time characteristics of the apparent slow wave.

Manuscript received April 13, 1998; accepted July 1, 1998. Work supported by the ONR Ocean Acoustics Program.

The author is with Sonoquest Advanced Ultrasonics Research, Wellesley Hills, MA 02181-0001 (e-mail: chamuelj@ultranet.com).

II. Hypothesis

The hypothesis given is that the anomalous ultrasonic slow wave [2] is the result of multiple conversion of near-grazing underwater acoustic waves incident on a sandy bottom with depth-dependent elastic properties. The shear wave velocity of underwater unconsolidated sand increases rapidly with depth [14] in the upper few centimeters forming a strong velocity gradient layer 5 to 15 cm thick. An underwater acoustic wave incident at angles greater than the compressional wave critical angle is partially converted into a shear wave in the sandy bottom. The presence of the large shear velocity gradient couples the shear and compressional waves at different depths. It is known that the elastic properties of sand vary continuously with depth. The sand will be represented here with an approximate layered elastic model having only shear wave velocity variation with depth and a constant compressional wave velocity. Wave refraction depends on velocity ratios, and wave conversion efficiency depends on both density ratios and velocity ratios. The purpose of this preliminary study is to focus on propagation time characteristics.

III. Hypothetical Model Parameters

A sound source is located in water at distance h above the sand interface. A receiver is buried in the sand at depth d. The horizontal distance between source and receiver is x. The sand is modeled as three parallel elastic layers over a half-space. The compressional wave velocity c_p is 1700 m/s in all the sand layers. The shear wave velocity is 60, 140, 190, and 220 m/s consecutively starting from the top layer. The respective layer thicknesses are 4.5, 5.5, 6, and $\propto$ cm. The assumed shear wave velocities as a function of depth are higher than that reported for a typical sand bed. The shear wave velocity was not given directly by Boyle and Chotiros [3]. They mentioned that the shear wave velocity of sandy sediments similar to that used in their experimental tank is about 150 m/s. The sediment settled for 18 years under 3 m of water in the tank, and it may be possible that the shear wave velocity is higher than 150 m/s. The preliminary hypothetical model described above used shear velocities between 60 and 220 m/s to come up with one simplified layered elastic model matching the propagation time characteristics observed at different receiver depths.

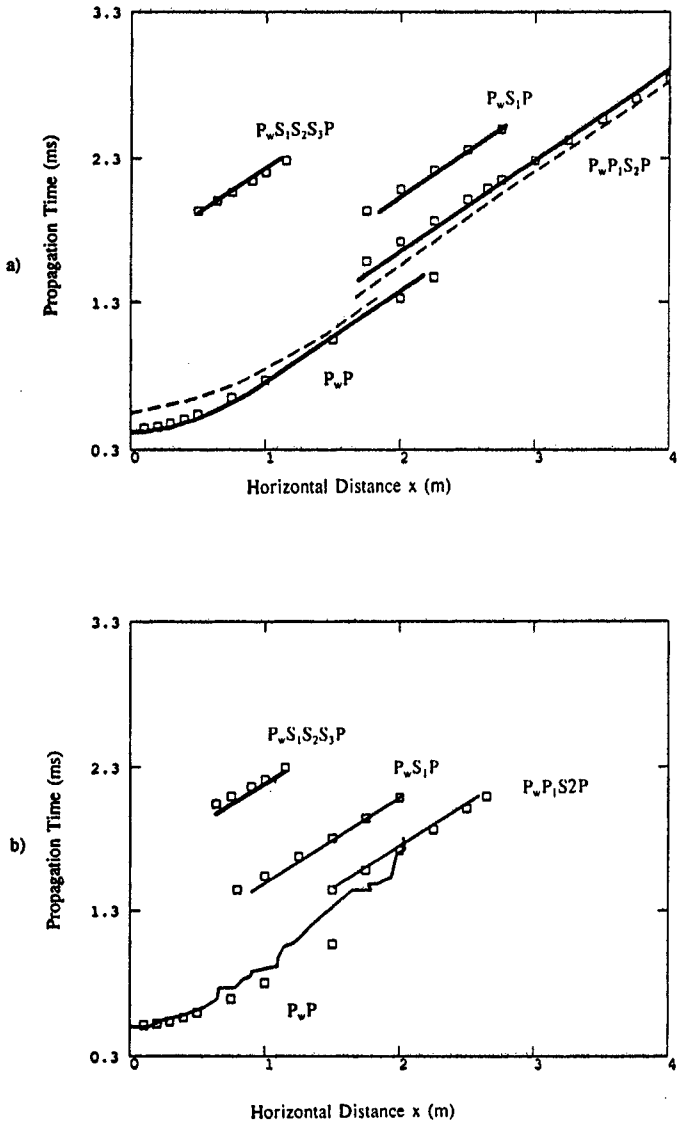

Fig. 1. Propagation time plotted as function of x. Open squares: Calculated results from a three-layered elastic model, (a) $d = 0.23$ m, and (b) $d = 0.35$ m. Solid lines: Experimental data by Boyle and Chotiros [3] replotted from their Figs. 6 and 7 ($d = 0.33$ m and 0.614 m). Dashed lines: Simulated numerical results by Kibblewhite and Wu [6] using Chotiros' modified Biot parameter values for $d = 0.33$ m.

IV. Results and Discussions

The salient features of the experimental propagation time plots by Boyle and Chotiros [3] were digitized and replotted to facilitate their comparison with calculated results from the proposed hypothetical model. Four distinct coexisting travel times were observed in the experimental propagation time plots (see Fig. 1). Corresponding numerical results by Kibblewhite and Wu [6] based on Biot parameters modified by Chotiros [2] are also plotted in Fig. 1(a). The Kibblewhite and Wu [6] explanation resulted in two rather than four coexisting travel times. The correct hypothetical model should explain the anomalous slow acoustic wave [3] and predict the four coexisting travel times in the experimental data [3].

The values of source height h and receiver depth d used in the calculations were determined directly from the experimental propagation time plots in [3] and not from the presumed values given by Boyle and Chotiros [3] because of several discrepancies between the measured and expected propagation time. For example, the value of h was determined from the arrival time t of the wave onset and not from the arrival time of the peak (displayed in Fig. 4 in [3]). Using $c = 1489$ m/s and $t = 302$ μs from the experimental plot, h equals $1489 \times 302 \times 10^{-6} = 0.45$ m instead of the given 0.49 m in [3].

Calculated results from the hypothetical layered elastic model are presented in Figs. 1(a) and (b) for two cases $d = 0.23$ m and $d = 0.35$ m corresponding to the experimental results (Figs. 6 and 7 in [3]), respectively, where the given values of d were 0.33 m and 0.614 m. The two receiver depths used in the calculations were determined from the arrival time $t = 458$ μs and $t = 517$ μs of the wave onset at $x = 0$ (Figs. 6 and 7 in [3]), $h = 0.45$ m, $c = 1489$ m/s, and $c_p = 1700$ m/s. Note that the receiver depth was misprinted as 0.8 m instead of 0.08 m (in Fig. 5 of [3]). Propagation time for selected wave components were calculated using Snell's law. The notation used is as follows: subscript w represents waves in the water, and no subscript means that the compressional P wave or the shear S wave components remained of the same wave type (no conversion) for the remainder of the wavepath. For example, $P_wS_1S_2P$ represents a P wave in water converting into shear waves in the first and second layers and propagating the remainder of the path as a compressional wave. The calculated results were superimposed on the propagation time plots by Boyle and Chotiros [3]. The four sets of curves in Figs. 1(a) and 1(b), from bottom to top, represent the converted P_wP, $P_wP_1S_2P$, P_wS_1P, and $P_wS_1S_2S_3P$ components, respectively, for both cases $d = 0.23$ m and $d = 0.35$ m. Calculated propagation time results obtained from a single approximate layered model simultaneously matched all of the experimental multiple propagation time features presented in [3] for different source/receiver geometries. The preliminary hypothetical layered model presented here is not unique; it was presented simply to demonstrate that multiple wave conversion also can provide an explanation for the anomalous wave without contradicting the classic Biot parameter values for sand. Other more elaborate five-layer and seven-layer elastic models were also obtained by the author matching the experimental results by Boyle and Chotiros [3]. The effect of continuous velocity gradient in the sand and the relative amplitudes of the converted wave components in underwater sand will be discussed in a separate paper.

References

[1] T. G. Muir, C. W. Horton, and L. A. Thompson, "The penetration of highly directional acoustic beams into sediments," *J. Sound Vib.*, vol. 64, pp. 539–551, 1979.

[2] N. P. Chotiros, "Biot model of sound propagation in water-saturated sand," *J. Acoust. Soc. Amer.*, vol. 97, pp. 199–214, 1995.

[3] F. A. Boyle and N. P. Chotiros, "Experimental detection of a slow acoustic wave in sediment at shallow grazing angles," *J. Acoust. Soc. Amer.*, vol. 91, pp. 2615–2619, 1992.
[4] R. A. Altenburg and N. P. Chotiros, "Plane-wave analysis of acoustic signals in a sandy sediment," *J. Acoust. Soc. Amer.*, vol. 89, pp. 165–170, 1991.
[5] M. A. Biot, "Theory of propagation of elastic waves in a fluid-saturated porous solid: II. Higher frequency range," *J. Acoust. Soc. Amer.*, vol. 28, pp. 179–191, 1956.
[6] A. C. Kibblewhite and C. Y. Wu, "A study of reflection loss. II. Involving a porous layer and a demonstration of the Biot slow wave," *J. Acoust. Soc. Amer.*, vol. 96, pt. 1, pp. 2981–2992, 1994.
[7] R. D. Stoll, "Comments on Biot model of sound propagation in water-saturated sand," *J. Acoust. Soc. Amer.*, vol. 103, pp. 2723–2725, 1998.
[8] M. J. Buckingham, "Theory of compressional and shear waves in fluidlike marine sediments," *J. Acoust. Soc. Amer.*, vol. 103, pp. 288–299, 1998.
[9] F. B. Jensen and H. Schmidt, "Subcritical penetration of narrow Gaussian beams into sediments," *J. Acoust. Soc. Amer.*, vol. 82, pp. 574–579, 1987.
[10] A. Maguer, S. Fioravanti, and A. Lovik, "Below critical angle detection of buried objects," in *Proc. Oceans 1997 MTS/IEEE*, vol. 1, 1997, pp. 512–517.
[11] E. I. Thorsos, D. R. Jackson, J. E, Moe, and K. L. Williams, "Modeling of subcritical penetration into sediments due to interface roughness," in *NATO SACLANT Conf. Proc. on High Freq. Acoust. in Shallow Water*, Lerici, Italy, June 1997.
[12] R. A. Stephen and S. T. Bolmer, "The direct root in marine seismology," *Bull. Seism. Soc. Amer.*, vol. 75, pp. 57–67, 1985.
[13] T. Yamamoto, M. Kuru, and T. Nye, "Imaging the hydraulic structure of the seabed through crosswell acoustic tomography," *J. Acoust. Soc. Amer.*, vol. 100, pt. 2, p. 2764, 1996.
[14] M. Kimura and S. Kawashima, "Depth dependence of shear wave velocity in sands," *Jpn. J. Appl. Phys.*, vol. 34, pt. 1, no. 5(B), pp. 2936-2939, 1995.

1.2 Experimental Results on Refracted Converted Waves

Ultrasonic modeling techniques [19-22] were used to obtain qualitative and quantitative experimental results under controlled laboratory conditions. An experiment was first conducted to see if a slow Biot wave or a 1200 m/s "anomalous" wave could be detected in water-saturated sand. The experimental model consisted of a 10 cm diameter thin walled plastic tube filled with water-saturated sand. Source and receiver transducers were placed at a depth of 43 cm below the sand surface. The source was excited with a broadband pulse. The received waveform was displayed on an oscilloscope with a horizontal time scale of 20 us/div. The results showed only one compressional wave propagating with a velocity of 1652 m/s as shown in Fig.6. The waveform did not reveal a Biot wave or the "anomalous" 1200 m/s slow compressional wave.

The effect of continuous shear wave velocity increase with depth in water-saturated sand on refracted converted waves can be approximated using a discretely layered model. Fig. 7 illustrates refracted converted waves at a single solid/solid interface using a Lexan/Plexiglas experimental model. A shear wave incident from the Lexan generated a large refracted converted compressional wave "SP" in the Plexiglas. The model parameters are given in the figure. The measured elastic properties of the modeling materials are shown in parenthesis in the following order density, compressional wave velocity, and shear wave velocity. The Lexan/Plexiglas shear wave velocity ratio is 879/1367. Another similar experiment was conducted on a wax/Lexan interface with a smaller shear velocity ratio (600/879) also yielded a large shear/compressional conversion "SP" as shown in Fig. 8. In water-saturated sand, refracted converted waves are expected to occur at a much lower level. Preliminary refraction conversion results from water-covered sand could not be interpreted from the known fast compressional wave and shear wave velocities. The puzzling results led to redirecting the research to investigate the fundamental seismoacoustic properties of water-covered sand under various conditions as described in **SECTION 2**.

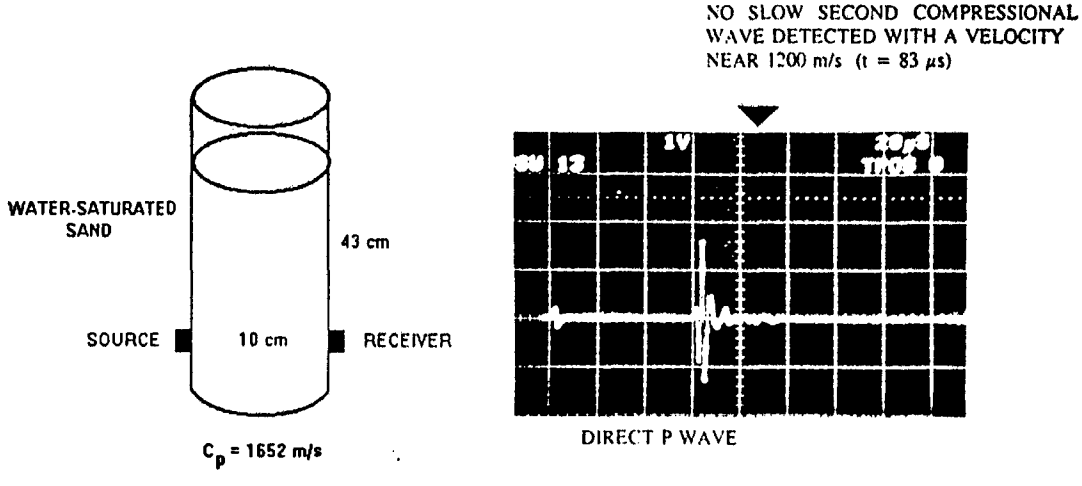

Fig. 6. Compressional wave in water-saturated sand.

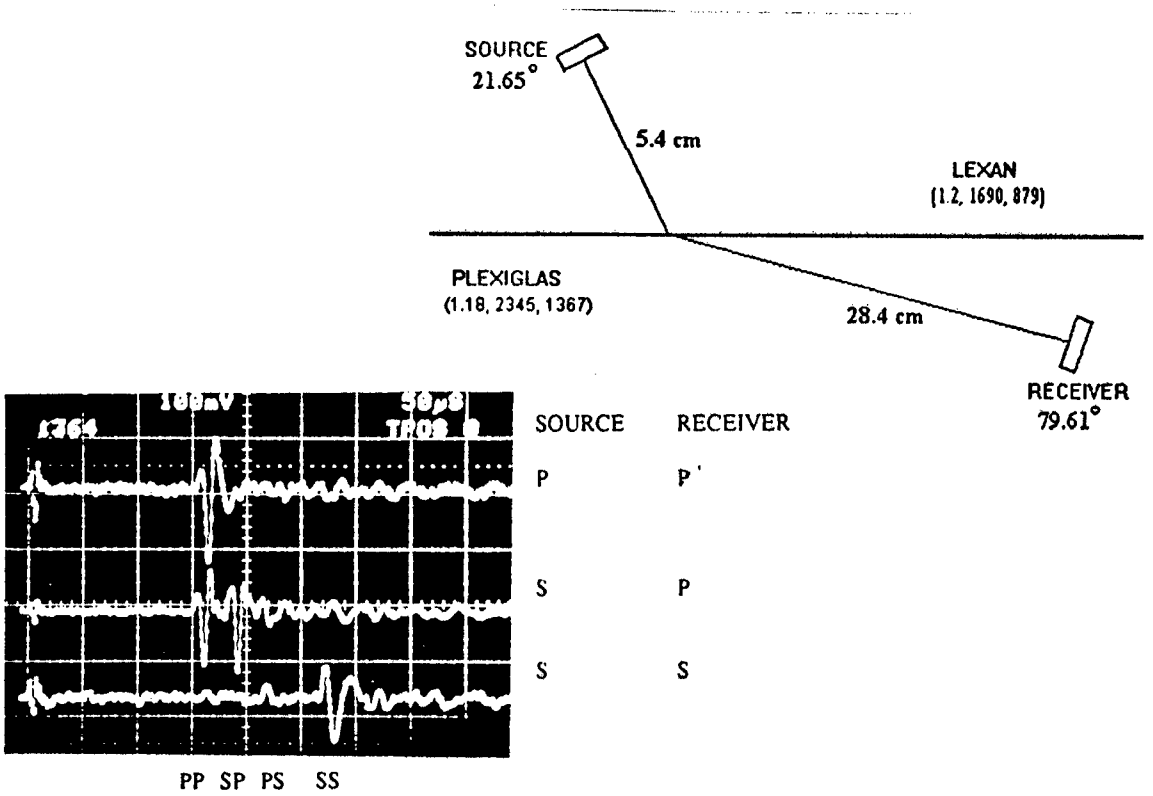

Fig. 7. Refracted converted waves in Lexan/Plexiglas model.

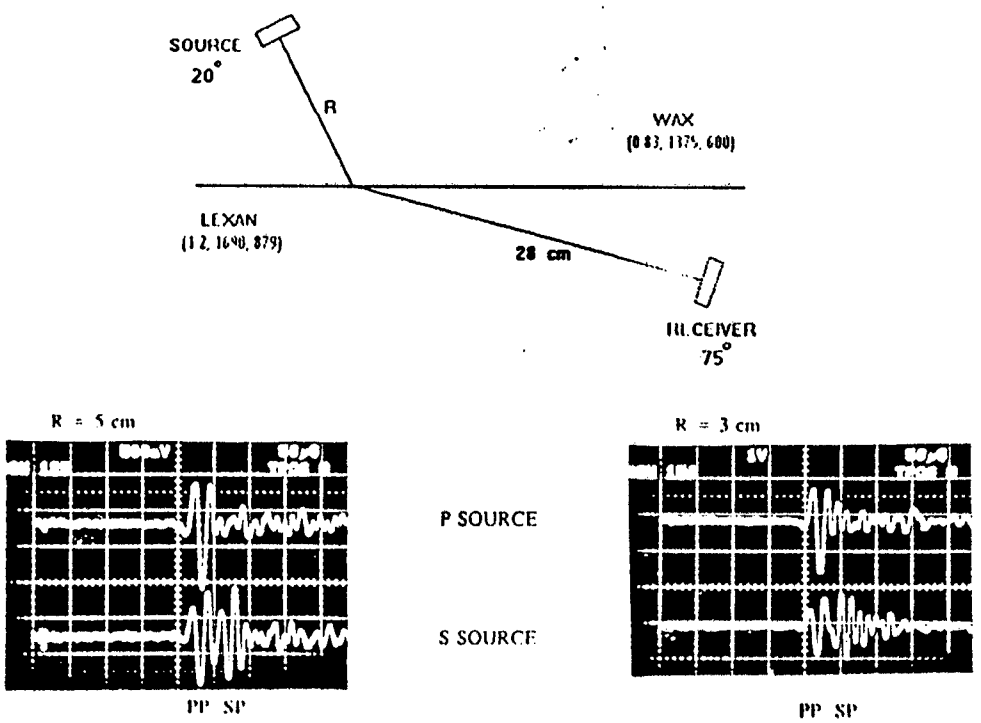

Fig. 8. Refracted converted waves in wax/Lexan model.

SECTION 2

2. Seismoacoustic Waves in Various Sand Conditions

While investigating the problem of refracted converted waves in water-covered sand, unexplained preliminary results were obtained that influenced the course of the research to acquire fundamental understanding of seismoacoustic properties of wet sand. These preliminary refraction conversion results could not be interpreted from the known fast compressional wave and shear wave velocities (Fig. 9). In this section, measured waveforms gathered from various sand conditions are presented.

First, here is a brief summary of the findings discussed in this section. Laboratory experimental results revealed the coexistence of a fast and a slow compressional wave in water-covered sand under certain conditions. The slow compressional wave had a time-varying dispersion and its velocity initially decreased with increasing water content, and increased with repeated stirring and compaction. The slow compressional wave was more detectable in disturbed sand and in coarse sand. It was surprising to observe that the velocity of the fast high-frequency compressional wave in water-saturated sand remained practically unchanged when the sand was drained. This indicated that the high-frequency components propagated through the sand grain matrix and were little affected by the drained water that existed in the pores. Current theories may need to be modified

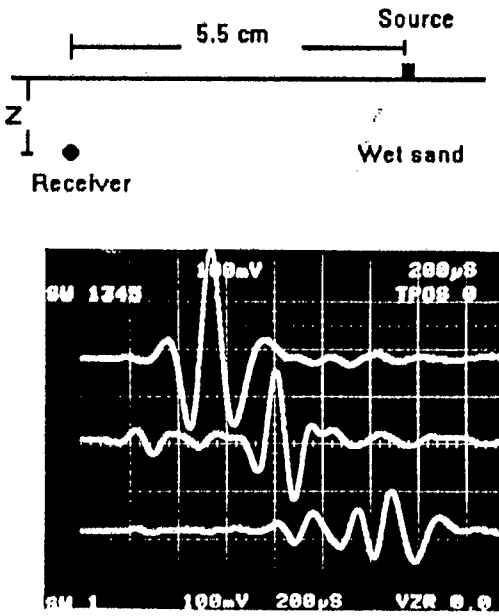

Fig. 9. Preliminary results showing waveforms in wet sand recorded at a fixed horizontal range (5.5 cm) and different receiver depth (0.25 cm, 3.25 cm, and 5.25 cm). Shear source and compressional receiver. Bottom trace shows dispersion and an unexplained refracted wave. Horizontal time scale 200 μs/div.

to account for this effect. Complete wetting of sand grains is not always achieved immediately upon immersing the sand in water resulting in unstable time-varying seismoacoustic properties. The new findings raised several questions that are presented in the CONCLUSION section.

Examples are given in Fig. 10 demonstrating typical variations in the received waveform from water-covered sand under various conditions. Fig. 10(a) shows a fast high-frequency compressional wave (1650 m/s) followed by a low-frequency shear wave (140 m/s) detected from naturally settled compacted sand. The waveforms in Fig. 10(b)-(e) were obtained from water-covered sand that was previously disturbed while the water level was below the sand. The high-frequency fast compressional wave was highly attenuated, and the shear wave remained practically unchanged. A new slow compressional wave (190-400 m/s) appeared in the disturbed sand arriving before the shear wave. Its amplitude and arrival time varied greatly depending on the effect of disturbance and trapped microbubbles. The source-receiver distance was 10 cm, and the source was excited with a single broadband pulse.

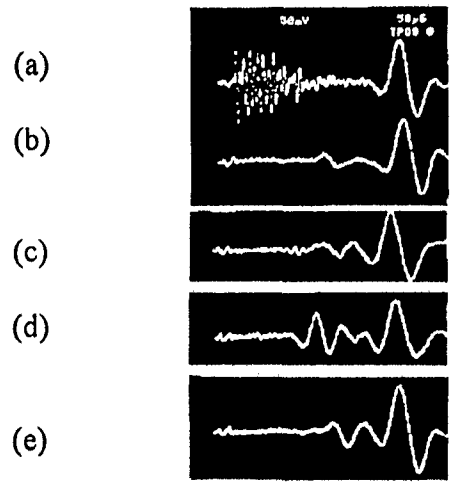

Fig. 10. Waveform variations in water-covered sand: (a) naturally deposited sand, (b)-(e) water-covered sand disturbed when water level was below sand. Notice presence of a high-frequency fast compressional wave 1650 m/s in (a) followed by a low-frequency shear wave 140 m/s. The fast compressional wave was highly attenuated in disturbed sand while the shear wave was practically not affected. A new slow compressional wave appeared in water-covered disturbed sand 190-400 m/s. Source-receiver distance was 4 cm. Time scale 50 μs/div..

Fig. 11 compares the waveforms of compressional waves in drained sand and water-covered sand. The compressional wave velocity in drained sand was 190 m/s with a 10 KHz center frequency. The waveform from the water-covered sand exhibited two compressional wave components consisting of a high-frequency fast compressional wave (~1650 m/s) and a slow low-frequency compressional wave. The shear wave velocity in drained sand was greater than the shear wave in water-covered sand (Fig.12). Variations in the shear wave amplitude and arrival time due to draining, saturation, liquefaction, and compaction are compared in Fig. 12(a)-(d).. The shear wave velocity decreased with liquefaction and water loading. The horizontal time scale was 200 μs/div.

Waveforms of the fast high-frequency compressional wave are examined in Fig. 13 using a 5 μs/div. time scale. The fast compressional wave velocity in water-covered naturally deposited sand was 1610 m/s (Fig. 13(a)). The velocity dropped from 1610 m/s to 1556 m/s with liquefaction Fig. 13(c). One surprising result was obtained when the water level was dropped 9 cm below the sand and the fast compressional wave did not change significantly (Fig. 13(b)). A similar experiment was conducted using sea water and it yielded the same surprising result (Fig. 14). The measured densities of the dry , water-saturated, and drained sand were 1765, 2169, and 2148 kg/m^3 , respectively.

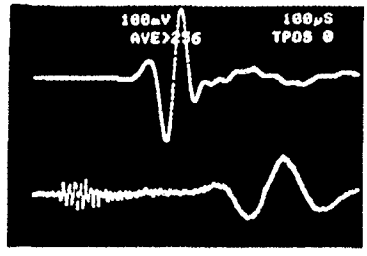

Drained Wet Sand

Water-covered

Fig. 11 . Comparison of compressional waves in drained wet sand and water-covered sand. The top trace shows a slow ~10 Khz compressional wave (190 m/s). The bottom trace shows two compressional waves one fast high frequency compressional wave and one slow low-frequency wave (faster than the shear wave). The source was excited with one broadband pulse. Time scale 100 μs/div..

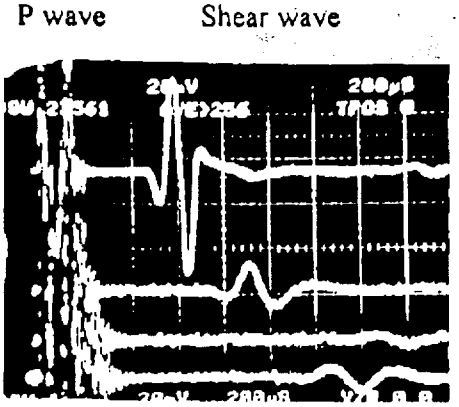

Fig. 12. Variations of shear wave amplitude and arrival time in naturally deposited underwater sand due to liquefaction and compactness. The high-frequency components at the beginning of the traces are due to compressional waves. Notice shear wave velocity decreased with liquefaction and water loading. Compaction increased the shear wave velocity of the previously liquefied sand. Source-receiver distance 4.7 cm at 2 cm depth. Horizontal time scale 200 μs/div..

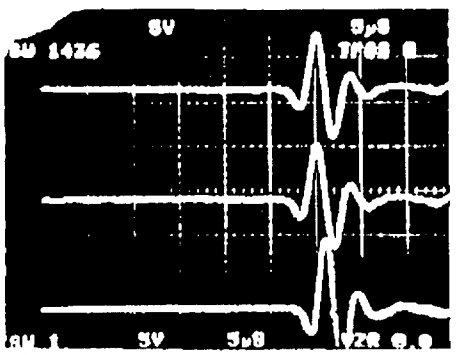

Fig. 13. Comparison of high-frequency compressional wave in sand. Compressional wave velocity dropped from 1610 m/s to 1556 m/s with liquefaction. Compressional wave attenuation decreased in liquefied sand. Horizontal time scale 5 μs/div.

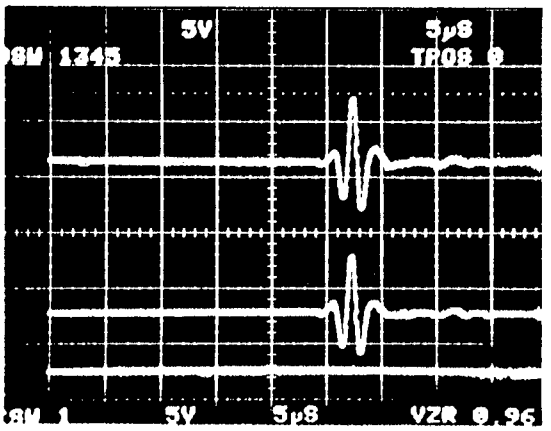

(a) Water-saturated

(b) Drained

Fig. 14. Surprising results showing the fast high-frequency compressional wave velocity (1750 m/s) in water-saturated sand (sea water) remained practically unchanged (dropped to only 1676 m/s) when the sea water was drained and the sand was sponge-dried. Source-receiver horizontal separation distance was 4 cm.

The center frequency of the broadband pulse used to excite the source was selected to enhance low or high frequency components in different experiments. The fast compressional wave in water-saturated sand (Fig. 15(b)) is compared with the compressional wave in water (Fig. 15(a)) using a 400 KHz pulse center frequency. The propagation distance was 3.3 cm.

The high-frequency fast compressional wave results presented in Fig. 13(b) and Fig. 14(b) were surprising because the compressional wave velocity in drained sand should be about 8x slower than the velocity in saturated sand [17-18] measured near 10 KHz. In order to reverify the results, another controlled experiment was conducted to measure the fast compressional wave in a small wet sand sample 1 x 2 x 4 cm as shown in Fig. 16. The procedure was as follows: source and receiver transducers were positioned in the middle of a water tank. The distance between the transducers was fixed at 4 cm. Sand was sprinkled very slowly over the water to form naturally settled sand. The tank wall was tapped periodically to compact the sand untill the tank was filled with water-saturated sand. The source was excited wih one broadband pulse. The received fast compressional wave was captured on the oscilloscope. The excess water on the sand surface was removed, and the sand was carved out from all the tank except for a rectangular sample 1 x 2 x 4 cm naturally held between the parallel faces of the transducers. During the carving process, the received fast compressional wave was monitored and it did not change. The sample was resaturated and the compressional waveform was recorded as shown in the top trace of Fig. 16. The measured compressional wave velocity was 1675 m/s. The second trace was obtained after sponge drying the sand sample. Notice that the compressional wave time of arrival remained almost unchanged. The sand sample was allowed to dry using blowing air on the sample. As the sample was drying, the received waveform was recorded periodically. The bottom trace in Fig. 16 was obtained from the

"almost dry" sample as the sand bar crumbled. This experiment confirmed that the compressional wave velocity of high-frequency components above 80 KHz remained close to the water-saturated velocity and did not decrease by a factor of eight. It seems that the high-frequency waves propagated in the naturally settled compacted sand as in a consolidated matrix not significantly affected by the drained water. Theoretical models and selected Biot parameters need to account for the compressional wave behavior decribed above [7-8, 25].

Bachrach and Nur [25] calculated the compressional wave velocity as function of water saturation in sand based on the Biot-Gassman prediction. The calculated results show that the compressional wave velocity initially decreases as the water content is increased, and then it starts to increase above 85% water saturation. At 99% water saturation, the compressional wave velocity is still less than 200 m/s. According to the theoretical model, the last 1% of water saturation increases the compressional wave velocity by almost a factor of 8.

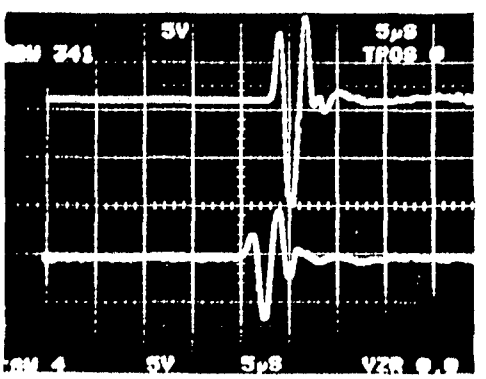

(a) Water

(b) Saturated Sand

Fig. 15. Received compressional wave in water (top trace), and in water-saturated sand (bottom trace). The distance between source and receiver was 3.3 cm.

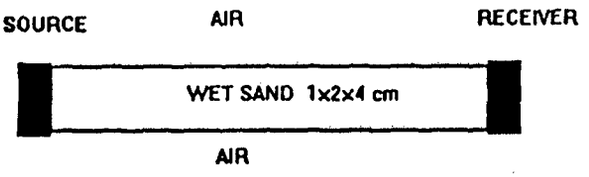

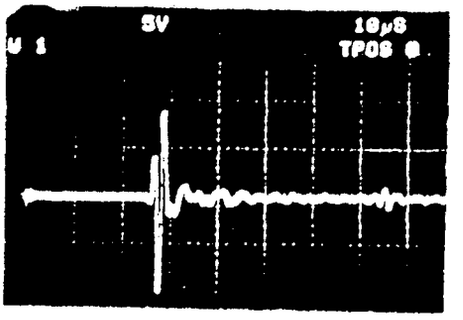

WATER SATURATED
C = 1675 M/S

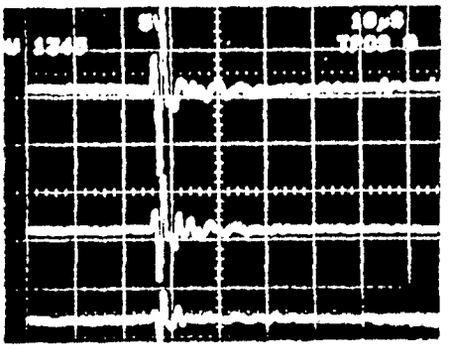

SPONGE DRIED

AIR BLOW DRYING BEGINS

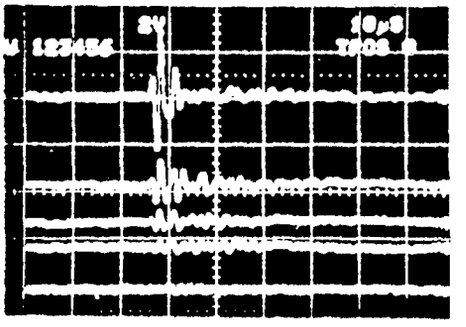

ALMOST DRY

Fig. 16. Effect of decreasing water content in wet sand on compressional wave . Waves propagated and detected in a wet sand block 1x2x4 cm carefully carved from naturally deposited sand. The compressional wave velocity remained almost constant as the water content decreased over a wide range of moisture content. Source-receiver distance 4 cm. Horizontal time scale 10 μs/div.

The arrival time of the slow compressional wave relative to the shear wave is shown in Fig. 17, where shear source and receiver transducers were utilized. Fig. 17(a) shows the slow compressional wave arriving before the shear wave in sprinkled compacted sand. When the sand was liquefied, the slow compressional wave amplitude decreased and new high-frequency components appeared in Fig. 17(b). Experiments using different types of sand were conducted. The slow compressional wave was observed more easily in coarse sand than in fine sand. Waveforms from coarse and fine sands are compared in Fig. 18.

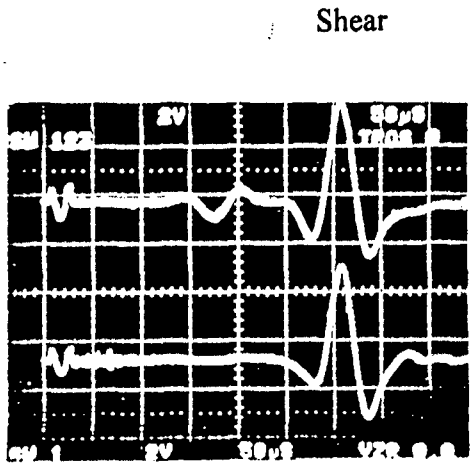

Fig. 17. Relative arrival times of compressional and shear waves in water-covered sand obtained using shear transducers. Source-receiver distance was 3 cm. Time scale 50 μ/div..

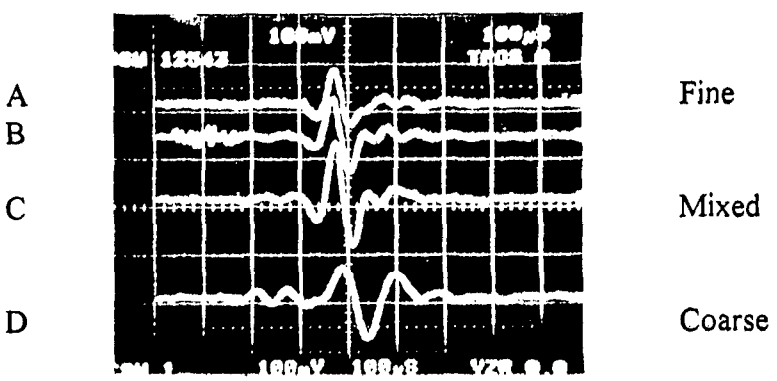

Fig. 18. Comparison of waveforms (A, C, and D) from water-covered near-saturated fine sand, coarse sand, and mixed sand, respectively. Trace B was obtained from near-saturated naturally settled mixed sand. Shear transducers were used, source-receiver distance was 4 cm. Horizontal time scale 100 μs/div..

Examples on the effect of repeated liquefaction and compaction on compressional waves in water-covered sand are given in Fig. 19 and Fig. 20. The source pulse waveform is displayed on the left portion of Fig. 19. With successive liquefaction and compaction, the amplitude of the high-frequency fast compressional wave increased, and the velocity of the dispersive slow compressional wave also increased (trace sequence from top to bottom). The bottom waveform in Fig. 20 shows how the slow low-frequency compressional wave overlapped a portion of the fast compressional wave as its velocity increased with repeated liquefaction and compaction.

It was also observed that the characteristics of compressional waves in water-covered sand vary with time (Fig. 21 and Fig. 22). Fig. 21 compares the waveforms at 5 minutes and 65 minutes following settling and compaction of the sand. The velocity of the slow compressional wave decreased with time. Stirring and compacting the sand increased the velocity of the slow compressional wave as demonstrated in Fig. 21(c).

The appearance of the slow compressional wave in water-covered sand sometimes occurs after waiting several seconds (~ 30 seconds) as shown in Fig.23. The exact cause has not yet been determined, however, it may be due to the formation of bubbles, settling of fine particles, or changes in grain to grain contact.

The observed slow compressional wave in water-covered sand is dispersive. Measured dispersion results are presented in Fig. 24 for play sand, and in Fig. 25 for silica sand (150 μm-425 μm). The measured dispersion characteristics are time dependent. The results shown in Fig. 25 were obtained 30 minutes after settling and compaction of the sand. Quantitative studies are needed to characterize the spatial distribution of water content, grain to grain wetting contact conditions, and microbubbles content. The Biot wave has not yet been identified in water-saturated sand. Hickey and Sabatier [31] reported on the dispersion of a slow compressional wave in air-filled sand.

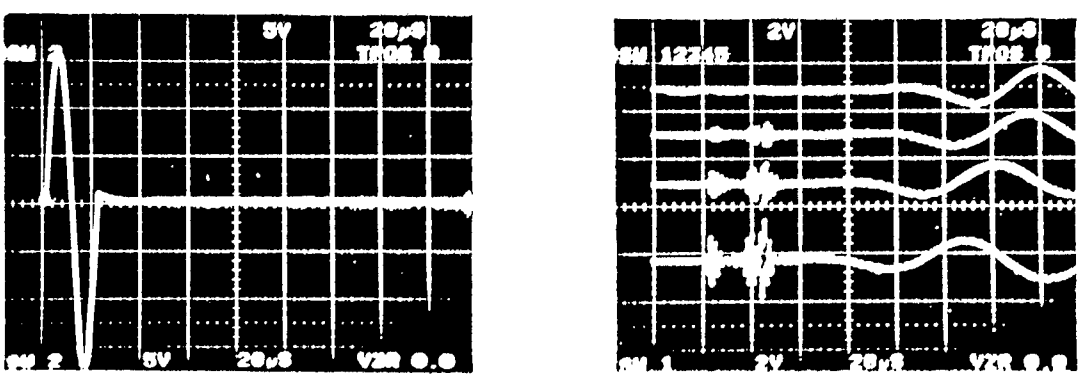

Fig. 19. Effect of repeated liquefaction and compaction on compressional waves in water-covered sand (x = 3 cm). The source broadband pulse waveform is shown on the left.

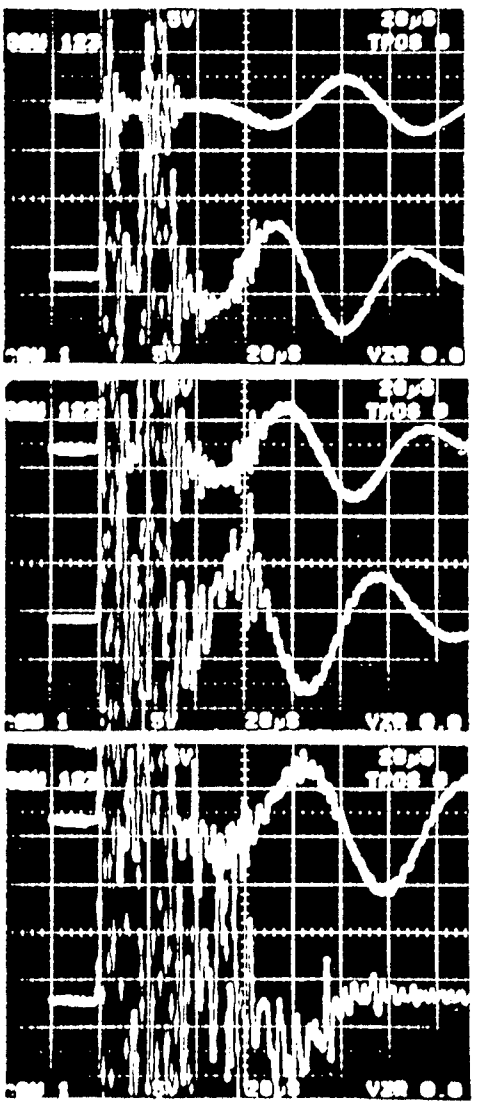

Fig. 20. Another example showing effect of repeated liquefaction and compaction on compressional waves in water-covered sand (x = 3 cm). Time scale 20 μs/div..

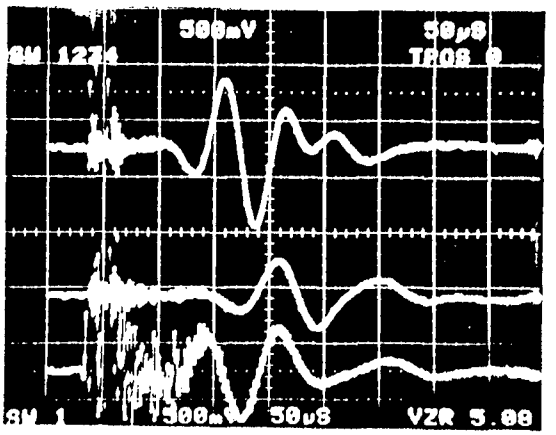

(a) t = 5 min.

(b) t = 65 min.

(c) t = 65 min.
+ Stirred and Compacted

Fig. 21. Effect of wetting time and disturbance on compressional waves in water-covered silica sand (425 μm-850 μm). The dry sand was "rained" (sprinkled) over the water tank and was compacted. Time measurement began immediately after settling. Source-receiver range was 4 cm. Time scale 50 μs/div..

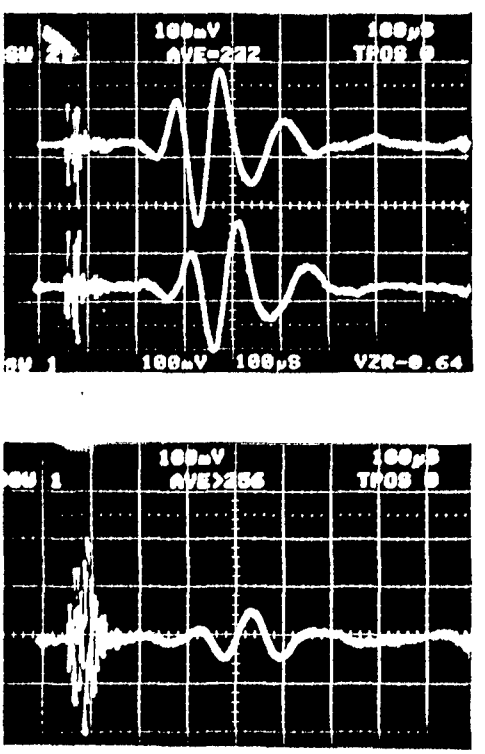

(a) t = 5 min.

(b) t = 65 min.

(c) t = 24 hours

Fig. 22. Aging effect on compressional waves in water-covered silica sand (425 μm-850 μm). Source -receiver distance was 6 cm. Horizontal time scale 100 μs/div..

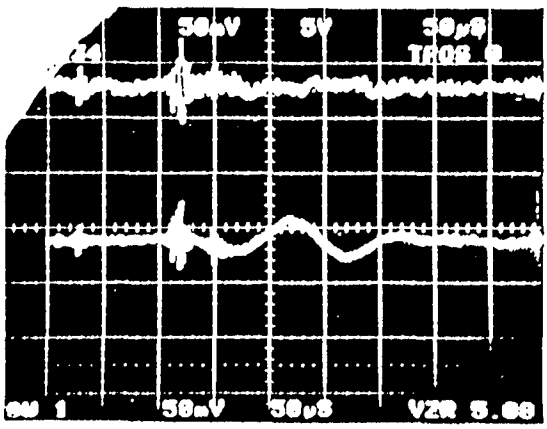

(a) t = 0

(b) t = 30 s

Fig. 23. Appearance of the slow compressional wave occurs sometimes after a waiting time of several seconds (~ 30 seconds) in water-covered sand, may be due to the formation of bubbles or settling of the fine particles. Source-receiver distance was 2.96 cm. Horizontal time scale 50 μs/div..

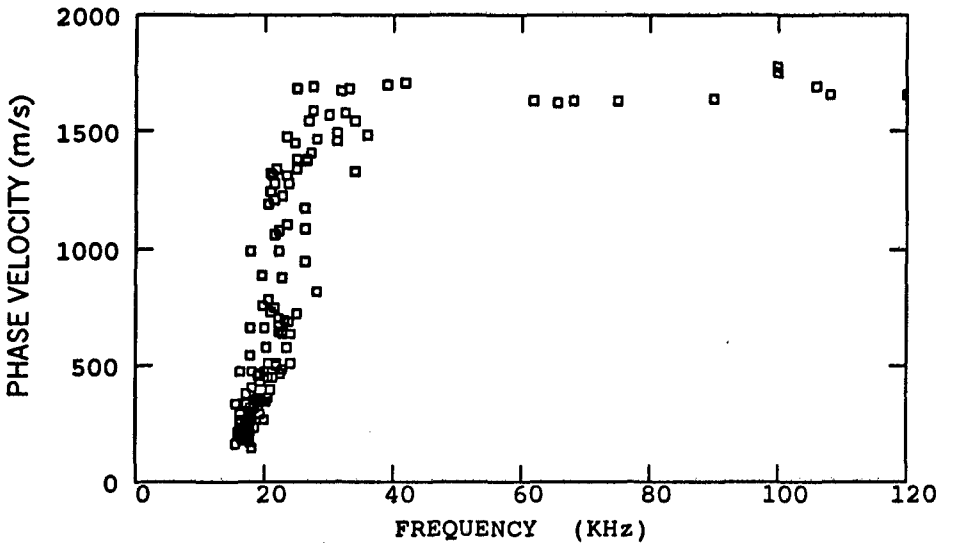

Fig. 24. Plot of measured dispersion of compressional wave phase velocity in water-covered play sand after substantial stirring and compaction. Vertical wave propagation path in sand.

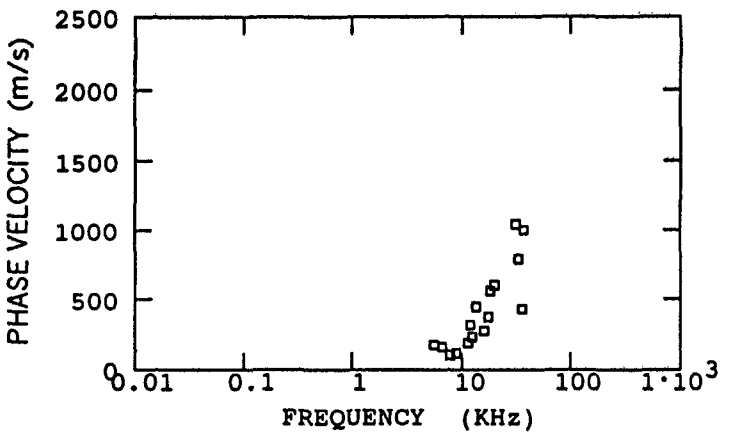

Fig. 25. Plot of measured dispersion of compressional wave phase velocity in water-covered silica sand (150 μm -425 μm) 30 minutes after settling and compaction. Vertical wave propagation path in sand.

SECTION 3

3.1 Effect of Water Level on Rayleigh and Shear Waves

Near the beach, variations in water level greatly affect the Rayleigh and shear waves. Laboratory experimental results on sand are presented in Fig. demonstrating variations in received waveforms as the water level changed. A piezoelectric source transducer was placed on the flat sand surface of drained wet sand to generate Rayleigh waves. A 2.5 cm diameter shear receiver transducer was buried at a distance of 10 cm flush with the sand surface and oriented horizontally to detect Rayleigh and shear waves. The Rayleigh wave in drained wet sand is shown in the top trace having a velocity of 65 m/s. The shear wave arrived a little before the Rayleigh wave and had a higher center frequency.

When the water level was increased to reach the sand surface, both the shear and Rayleigh wave amplitude and velocities decreased. The measured Rayleigh wave velocity in water-saturated sand was 44 m/s. Two other waveforms are presented in Fig. 26 with the water level at 1.5 cm and 3 cm below the sand surface. The ratio of shear wave velocity to Rayleigh wave velocity varied nonlinearly as the water level dropped. Notice as the water level dropped 3 cm below the sand surface, the Rayleigh wave amplitude (right peak) increased and its propagation time decreased. The wave velocities should increase with depth in sand, however, the presence of the water level at a short distance below the surface decreases the velocity of the lower frequency components reaching the deeper water-saturated sand. Future studies are needed to quantify these water level effects.

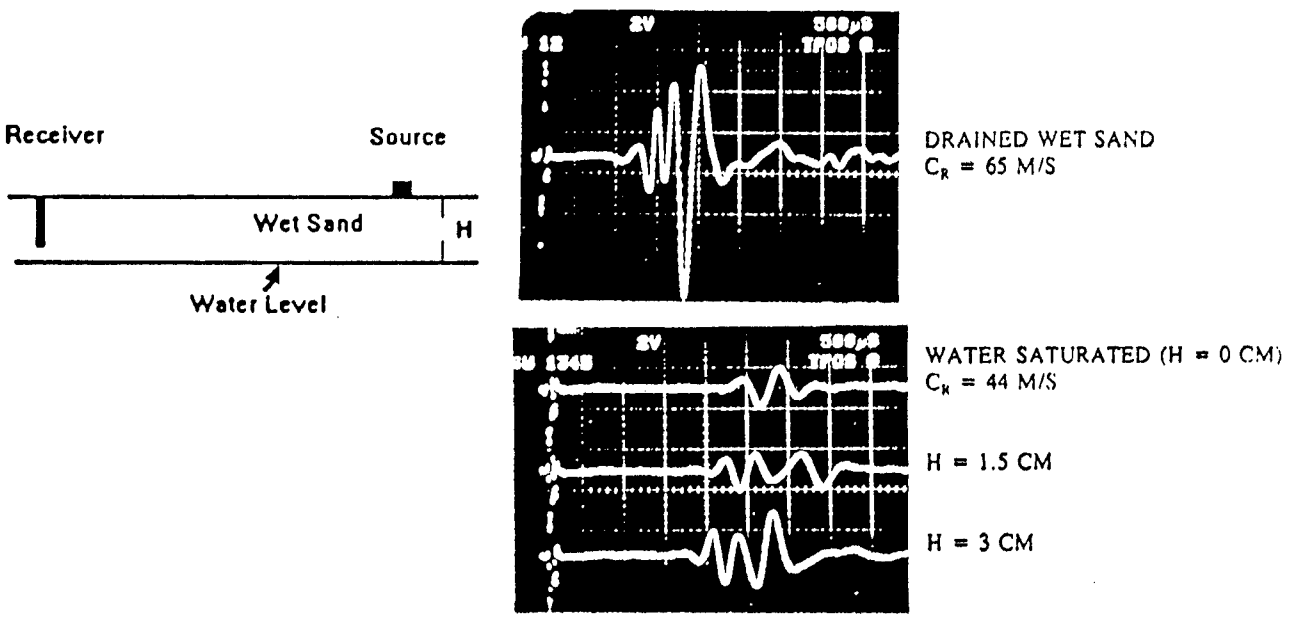

Fig. 26. Effect of water level in sand on Rayleigh and shear waves.

3.2 Conversion of Interface Waves Into Shear Waves by Water Edge

The conversion of interface waves into shear waves by a water edge is demonstrated. A water/Plexiglas laboratory ultrasonic model was used in the experiment. A 2 mm diameter piezoelectric transducer was placed on the flat suface of a Plexiglas block simulating an elastic half-space. A shear receiver was positioned 2 cm below the surface at a distance of 25.7 cm. Fig. 27 shows two waveforms obtained from the Plexiglas block partially immersed in water. The angle of intersection between the water and Plexiglas varied. The top waveform shows the direct shear wave "S1" followed by an unexpected large shear wave "S2"generated from partial conversion of the incident Rayleigh wave by the water edge. The angle of intersection was 90 degrees (ignoring the curved surface tension region). The distance between the source and the water edge was 18.7 cm. The bottom waveform was recorded with the block tilted to make a 10 degree angle of intersection. Again, a significant shear wave was generated by the conversion of the Rayleigh wave. Similar results were observed from the conversion of a Scholte wave into a shear wave by the water edge when the source was located underwater on the Plexiglas surface. The results hint the potential role of liquefied localized regions in seafloor on converting interface waves into shear waves contributing to transmission loss in very shallow water even in the absence of topography.

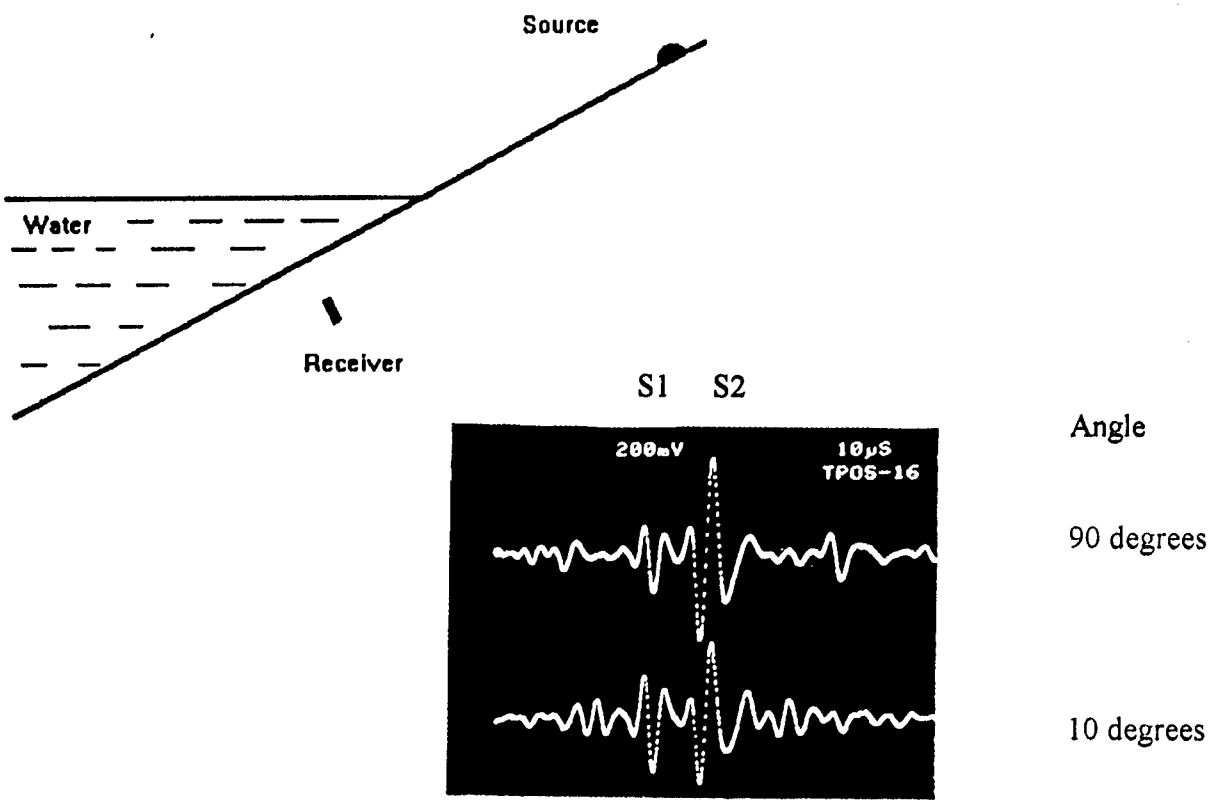

Fig. 27. Shear wave S2 generated in elastic bottom from the conversion of a Rayleigh wave interacting with the water edge. Horizontal time scale 10 us/div. Time at beginning of trace 160 us. S1 is the direct shear wave from source to receiver.

The presence of a water puddles on the surface of a solid can also partially convert an incident Rayleigh wave into shear waves. Fig. 28 shows the effect of varying the diameter of a single circular water puddle placed on a Plexiglas surface on converting an incident Rayleigh into a shear wave. The waveform was recorded with the puddle diameter 0, 5, 10, and 20 mm. Distance from source to puddle 18.7 cm. horizontal distance from puddle to receiver 7 cm, receiver depth 2 cm.

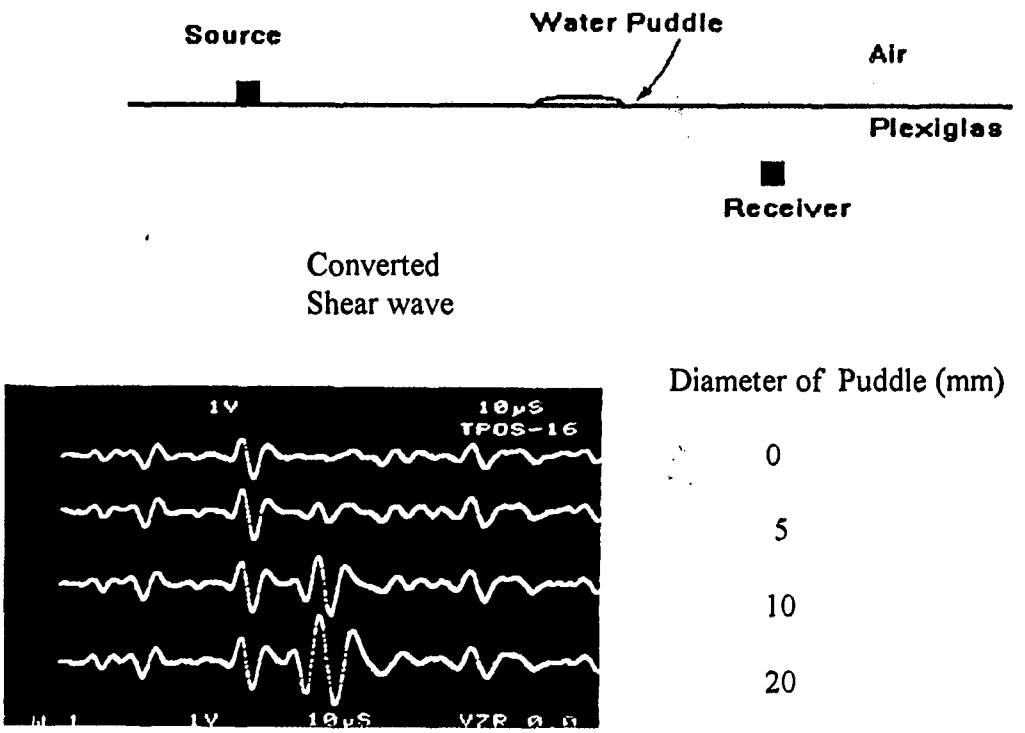

Fig. 28. Effect diameter of water puddle placed on solid flat surface (Plexiglas) on converting incident Rayleigh waves into shear waves penerating the solid.

3.3 On Coexistence of Rayleigh and Scholte Waves

A current controversial fundamental problem needs to be resolved regarding the coexistence of a Rayleigh wave and a Scholte wave at a fluid/solid interface when the fluid sound velocity is between the shear and compressional wave velocities in the solid [3] (e.g. sandy sediments, Plexiglas, sandstone). Padilla et al. [3] presented numerical results showing there might exist two surface waves from the roots of the dispersion equation and confirmed the existence of a Rayleigh wave and a Scholte wave from water/Plexiglas experimental results. In 1982, Chamuel [38] presented experimental results from an ultrasonic water/Plexiglas model indicating that only one interface Scholte wave exists at such interface using point source and receiver transducers placed on the interface.

In view of the findings presented in the previous section on the generation of shear waves from the conversion of Rayleigh waves by a water edge, the interpretation of the experimental results by Padilla et al. [3] from water/Plexiglas became questionable.

A new experiment was conducted using a water/Plexiglas model that provided an explanation for the excessive amplitude decay of the apparent "Rayleigh" wave component observed by Padilla et al. [3]. The new findings indicated that the experimental results in [3] were probably misinterpreted by referring to the converted shear wave as a Rayleigh wave coexisting with the Scholte wave. The Rayleigh wave from the free Plexiglas model in air is shown in the top trace of Fig. 29 (no separate shear wave component observed). A piezoelectric transducer (2 mm diameter) was placed on the surface of the Plexiglas to generate a Rayleigh wave. A shear receiver transducer was coupled to the end of the Plexiglas block . The distance between source and receiver was 14 cm. The middle trace shows two wave components (a shear wave and a Scholte wave) generated from the conversion of the Rayleigh wave by partial immersion in water wetting 5 cm length of the wavepath. Touching the surface of the Plexiglas attenuated the Scholte wave and did not disturb the shear wave generated from the water edge conversion as shown in the bottom trace verifying that the remaining unattenuated component was a body shear wave and not a surface wave. Spherical spreading of the shear wave accounts for the unexplained excessive amplitude decay of the apparent "Rayleigh" wave component observed by Padilla et al. [3]. The arrival time of the converted shear wave by the water edge decreased as the immersion length increased.

Fig. 30 shows the calculated arrival time of the Scholte wave and shear wave components generated by the conversion of the Rayleigh wave by the water edge. In the figure, the experimental results by Padilla et al.[3] are also replotted with the calculated arrival time of the hypothetical second Rayleigh wave. Notice the good match between the experimental results from Reference [3] and the new calculated results based on the converted shear wave. The calculated results were obtained using the following parameters: compressional wave velocity 2745 m/s, shear wave velocity 1363 m/s, Rayleigh wave velocity 1295 m/s, Scholte wave velocity 1058 m/s, range 14 cm, and receiver depth 3 mm (effective depth of shear receiver being on the side of the Plexiglas block). The findings are important for interpreting the roots of the dispersion equation and predicting energy partitioning in seismoacoustic signals in sandy sediments.

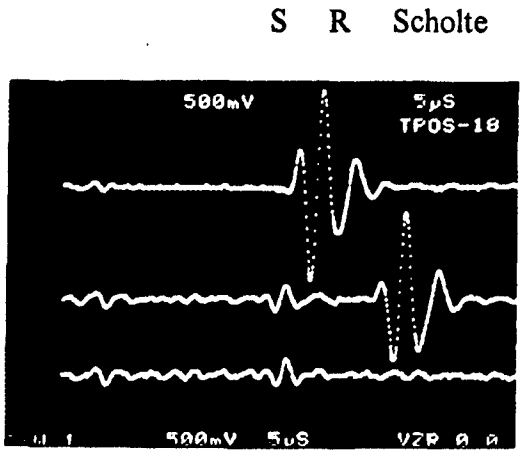

Rayleigh wave on free surface

Conversion into shear and Scholte waves by partial immersion in water

Touched surface to attenuate all interface waves demonstrating that the remaining component is a converted shear wave

Fig. 29. Experimental results demonstrating the conversion of a Rayleigh wave by partial immersion of a flat solid in water produces a Schote wave and a body shear wave and not a second interface wave as reported in [3].

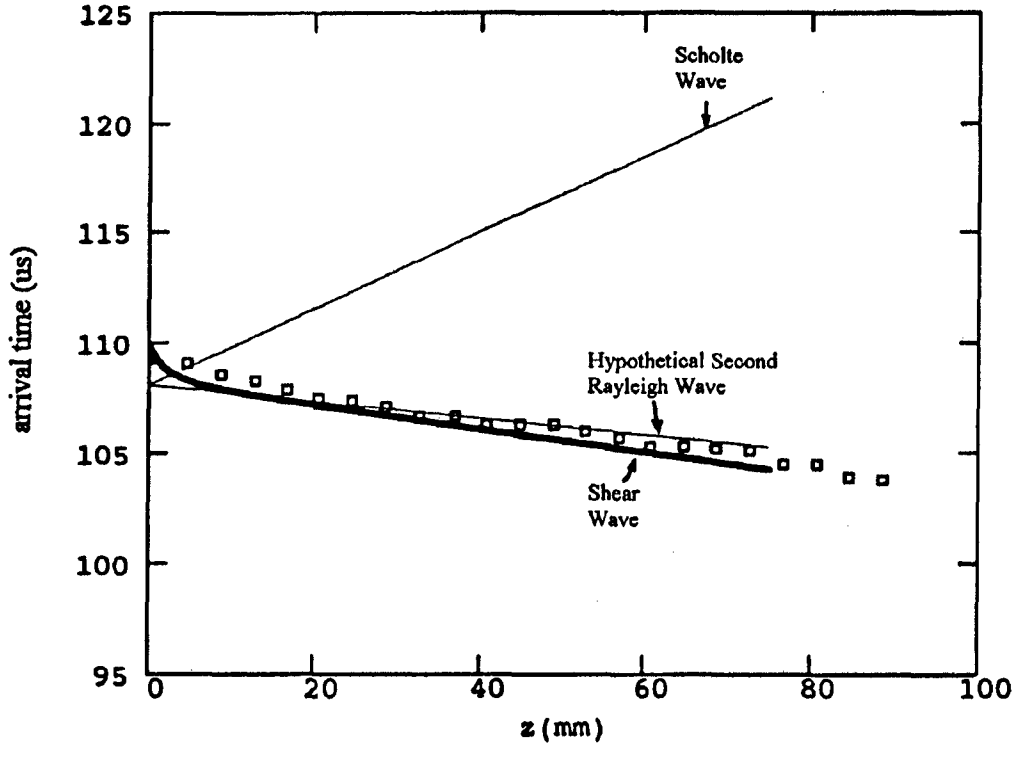

Fig. 30. Calculated arrival time of Scholte and shear waves generated from the conversion of a Rayleigh wave as a function of immersion length for a water/Plexiglas model. The experimental results by Padilla et al. [3] are plotted (open squares) together with the calculated arrival times of the hypothetical second Rayleigh wave (thin solid line).

SECTION 4. Ripples

4.1 Scholte Wave Dispersion by Rippled Liquid/Solid Interface Topography

Int. Congress Acoust. & 135th Meeting Acoust. Soc. Am., Seattle, June 1998

Scholte Wave Dispersion by Rippled Liquid/Solid Interface Topography

Jacques R. Chamuel

Sonoquest Advanced Ultrasonics Research, P. O. Box 81153, Wellesley Hills, MA 02181-0001

ict: Quantitative experimental results are presented characterizing the dispersion of Scholte waves propagating along led surface of an immersed "soft" solid half-space. One model has a sinusoidal profile with a ratio of corrugation ude to wavelength of 0.25. Scholte and Rayleigh wave experimental dispersion results are compared with numerical s on Rayleigh wave dispersion along a "hard" corrugated solid half-space [N.E. Glass, R. Loudon, and A. A. Judin, Physical Review B 24, 6843-6861 (1981)]. The findings reveal that a rippled "soft" liquid/solid interface can ase the velocity of high-frequency Scholte wave components propagating normal to the ripples by more than 70%.

INTRODUCTION

e effect of a rippled liquid/solid interface on the dispersion of Scholte waves is not known. Frequency-ndent multiple scattering phenomena occur as near-grazing underwater acoustic waves and Scholte waves act with periodic seafloor topography having dimensions comparable to the wavelength. In order to develop ical understanding of the interaction of broadband transient underwater acoustic waves and Scholte waves with pled ocean bottom, experimental ultrasonic experiments were conducted on immersed isotropic "soft" models a sinusoidally corrugated surface. Quantitative experimental results were obtained characterizing the dispersion Rayleigh and Scholte waves caused by a periodic liquid/solid interface.

MODEL EXPERIMENTS AND RESULTS

A sinuoidal pattern was machined along the edge of a 4.5 mm thick Plexiglas plate. The spatial wavelength of e periodic pattern was 2 cm and the peak-to-peak amplitude was 1 cm. The measured Plexiglas velocities were s follows: compressional plate velocity = 2313 m/s, shear wave velocity = 1344 m/s, flat edge Rayleigh wave elocity = 1220 m/s, flat edge Scholte wave velocity = 1109 m/s. The top trace of Figure 1(a) compares the ispersed waveforms of Rayleigh and Scholte waves propagating along the periodic surface. Rayleigh and Scholte vaves were obtained from air/Plexiglas and water/Plexiglas models, respectively. The Scholte waveform was stretched more to the right than the Rayleigh wave indicating that it was slower than the Rayleigh wave. The bottom trace of Figure 1(a) shows the arrival time of the corresponding Rayleigh wave along a flat surface (no

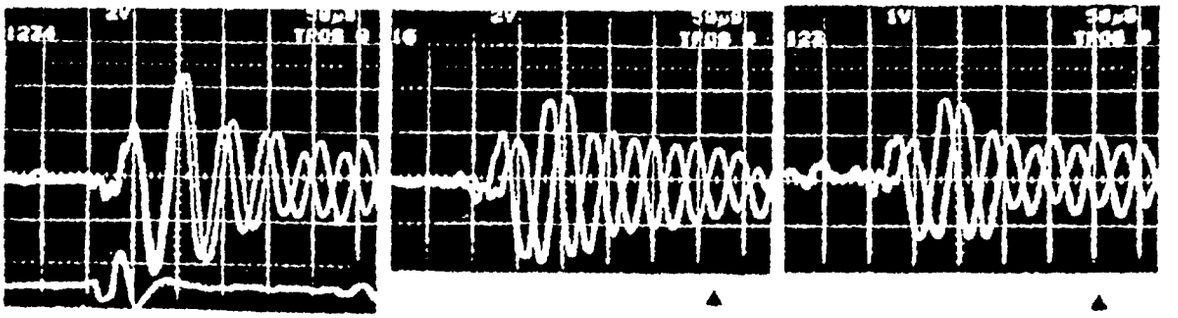

(a) (b) (c)

FIGURE 1. Comparison of received waveforms and arrival time; (a) Top Trace: Rayleigh and Scholte waves along corrugated surface (range x = 12 cm), Bottom Trace: reference Rayleigh wave from flat solid surface, (b) Rayleigh wave along corrugated surface detected at two positions separated by one corrugation cycle (2 cm), (c) Scholte wave along corrugated surface detected at the same two positions in (b).

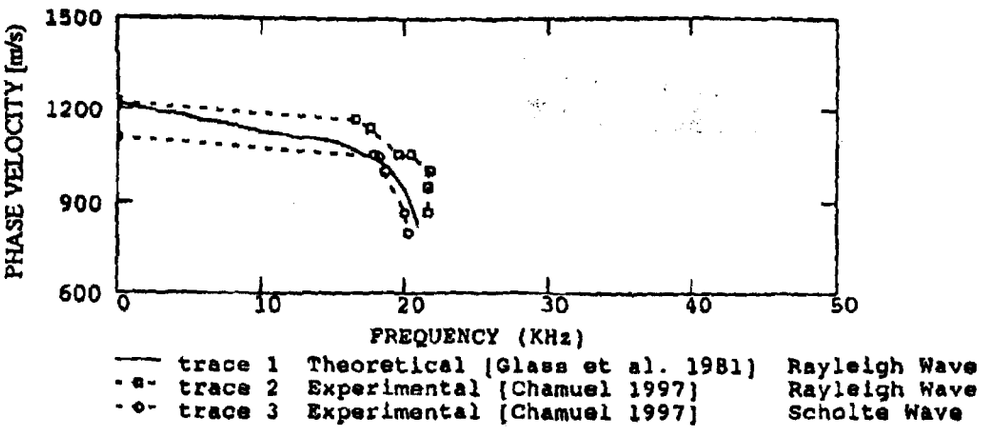

FIGURE 2. Rayleigh and Scholte wave dispersion experimental results compared with approximately scaled theoretical dispersion results by Glass et al. [1] on Rayleigh wave.

corrugation). Rayleigh and Scholte waves propagating along an isotropic elastic half-space are nondispersive. The source/receiver range was fixed at x = 12 cm. The vertical amplitude scale was arbitrary. Figure 1(b) compares the Rayleigh wave detected at two different locations separated by one cycle along the corrugation (x = 10 cm and x = 12 cm). The time delay between the two waveforms caused the corresponding Bragg frequency component to be shifted by 180° (arrow pointing to out of phase components). The measured Rayleigh wave Bragg frequency along this sinusoidal surface was 21.62 KHz. The periodic surface decreased the Rayleigh wave velocity from 1220 m/s to 865 m/s at the Bragg frequency. The corresponding Scholte wave experimental results, measured at the same two locations, are shown in Figure 1(c). The Scholte wave Bragg frequency was 20.2 KHz indicating that the Scholte wave velocity decreased from 1109 m/s to 808 m/s.

The Scholte and Rayleigh wave experimental dispersion results obtained from a "soft" elastic models are compared with replotted scaled numerical results [1] on Rayleigh wave dispersion for a "hard" corrugated solid half-space. The scaling was achieved by simply multiplying the dispersion curve by the Rayleigh wave velocity ratio between the theoretical "hard" model and the experimental "soft" model. This yields approximate results because Poisson's ratio was not changed. Figure 2 compares the Rayleigh and Scholte wave experimental dispersion results with scaled theoretical dispersion curve of Glass et al. The experimental results generally agreed with the Rayleigh wave theoretical results by Glass et al.. Work is in progress to compare the experimental results with Boström's calculated results [2] on Rayleigh waves. To the author's knowledge, there are no known published theoretical or numerical results characterizing the dispersion of Scholte waves by a large amplitude corrugated liquid/solid interface. Quantitative controlled laboratory ultrasonic measurements revealed that a rippled "soft" liquid/solid interface can decrease the velocity of high-frequency Scholte wave components propagating normal to the ripples by more than 70%. The findings indicate the potential importance of seafloor topography on acoustic inversion and detection of buried objects in shallow water.

ACKNOWLEDGEMENTS

Work supported by ONR.

REFERENCES

1. Glass, N. E., Loudon, R. and Maradudin, A. A., *Physical Review* B.24, 6843-6861 (1981).
2. Boström, A., *J. Acoust. Soc. Am.* 85 (4), 1549-1555 (1989).

4.2 Rayleigh Waveform from Rippled Drained Wet Sand Surface

The effect of a rippled wet sand surface on Rayleigh wave dispersion and attenuation is shown in Fig. 33. The top trace was obtained from a flat surface of a drained sand model. The water level was 9 cm below the sand surface. A compressional source was placed on the free wet sand surface to generate a Rayleigh wave. The receiver was a 2.5 cm diameter shear transducer horizontally oriented and buried flush with the sand surface to detect both shear waves and Rayleigh waves. The source-receiver range was 10 cm. The source was excited with a broadband pulse and generated a transient Rayleigh wave with a 3.1 KHz center frequency. The shear wave arrived before the Rayleigh wave and partially overlapped the Rayleigh wave. The shear wave center frequency was 5 KHz, and the Rayleigh wave velocity was 65 m/s. A sinusoidal corrugation was made on the wet sand surface with a 1 cm spatial wavelength and 0.25 cm amplitude. The sand ripples attenuated the Rayleigh wave and generated a dispersive wavetrain with a 2.32 KHz Bragg frequency [19]. The sand ripples decreased the effective Rayleigh wave velocity.

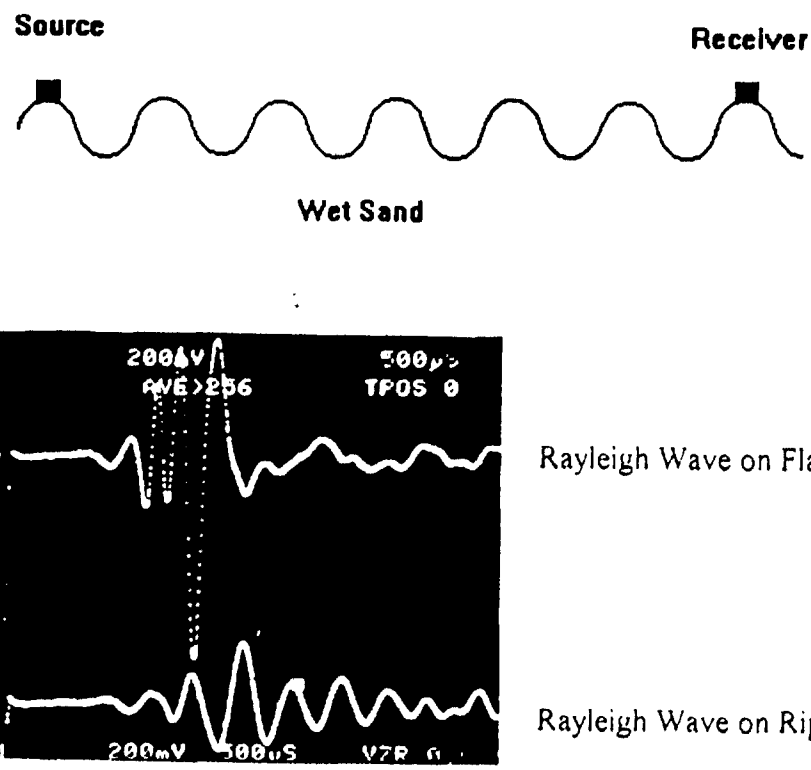

Fig. 33. Effect of sand ripples on Rayleigh wave dispersion. Corrugation spatial wavelength 1cm, ripple amplitude 0.25 cm, source-receiver distance 10 cm. Bragg frequency resonance 2.32 KHz.

SECTION 5

5. Wedge Waves Along Sand Dollar Skeleton Edge

In order to reliably detect and identify small buried objects in littoral sandy sediments using acoustic waves, it is essential to understand the seismoacoustic response of partially buried inclusions such as seashells and sand dollars. This section presents the first experimental results on wedge waves propagating along the edge of sand dollar skeletons. Ash et al. [34] suggested the presence of a slow edge wave along the tip of a triangular ridge. In 1972, Lagasse [35] discovered a *nondispersive* flexural edge wave propagating along the apex of a small angle elastic wedge using a numerical finite element approach. The same year, Maradudin et al. [36] independently presented theoretical results on edge modes in finite crystals. The wedge wave is a unique nondispersive flexural wave that propagates with a velocity that depends on the wedge apex angle according to Lagasse's empirical relation

$$V_m = C_R \sin m\theta$$

where V_m = antisymmetric mode velocity, C_R = Rayleigh wave velocity, m = mode number and θ = wedge angle. The number of antisymmetric edge modes is determined by the relation $m\theta < 90°$. These waves will be referred to here as "wedge waves" in order not to confuse them with the *dispersive* flexural edge waves along the edge of a plate. Chamuel [37] reported on edge waves along immersed elastic elliptical wedge with range-dependent apex angle. The sand dollar has the geometry of a wedge with a variable angle. A sand dollar skeleton is formed from two fused plates. Fig. 34 shows a sand dollar cross section revealing the wedge geometry near its edge. The wedge angle between the fused plates varies between 15°-18°. The edge is also rounded with a 1-4 mm truncation.

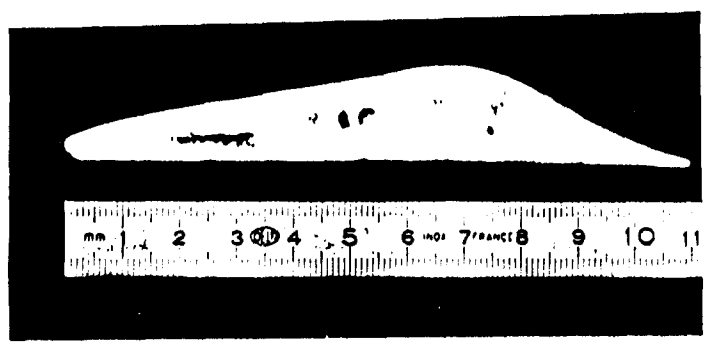

Fig. 34. Sand dollar skeleton cross section showing wedge geometry with variable edge angle.

The thickness of the sand dollar edge varies along the perimeter. Waveforms of wedge waves obtained from the thin and thick edge regions are compared in Fig. 35. Two superimposed sets of wedge waves are shown in the figure demonstrating the close similar elastic properties of sand dollars of the same age. This may be acoustically significant in single-age group sand dollar beds. The wedge wave velocity is greater along the thick edge portion

Waveforms from a 5.04 cm edge segment cut from a sand dollar skeleton with a diameter of 11.4 cm are compared in Fig. 36. The top trace was obtained with the source and receiver transducers oriented nearly parallel to the sand dollar edge. A longitudinal wave and a small edge wave were observed. The middle trace shows a symmetric Rayleigh edge wave obtained with the transducers oriented normal to the edge and parallel to the wedge center plane. The bottom trace shows a large antisymmetric flexural wedge wave generated and detected with the transducers normal to both the edge and center plane. The measured compressional, Rayleigh, and antisymmetric wedge waves velocities were 3702 m/s, 2311 m/s, and 1774 m/s, respectively.

Waveforms from whole uncut sand dollar skeletons are presented in Fig. 37. The wedge wave was detected at one location along the edge (top trace), and then the receiver was moved 9 cm further along the edge (bottom trace). The measured Rayleigh wave velocity was 2160 m/s and the wedge wave velocity varied along the wavepath from1572 m/s to 1647 m/s. Water loading decreased the wedge wave velocity and amplitude. Fig. 38 compares wedge waves from a sand dollar skeleton in air and in water. Further research is needed to characterize the seismoacoustic response of seashells and sand dollars.

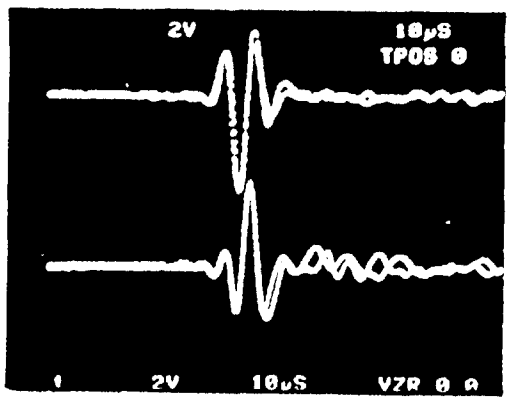

Thick Section

Thin Section

Fig. 35. Superimposed antisymmetric edge waves from two sand dollars with same size showing close similarity between their elastic properties.

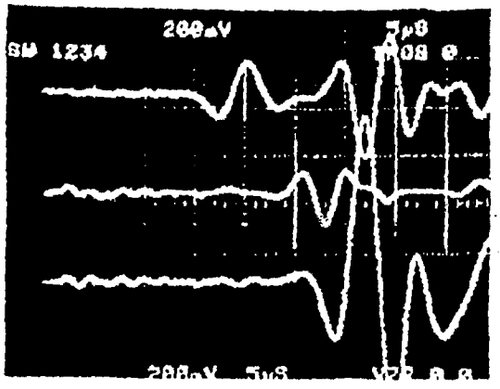

Fig. 36. Comparison of waveforms from a sand dollar edge segment 5.04 cm in length. Top: Longitudinal edge excitation . Middle: Normal symmetric edge excitation. Bottom: Antisymmetric flexural edge excitation.

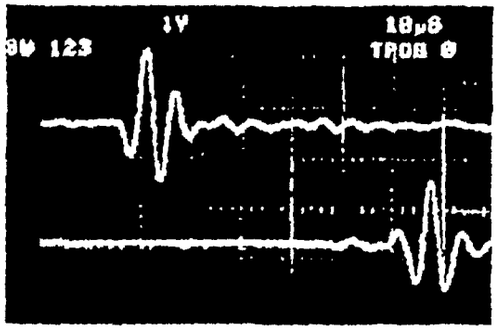

Fig. 37. Wedge wave detected at two locations separated by 9 cm along edge.

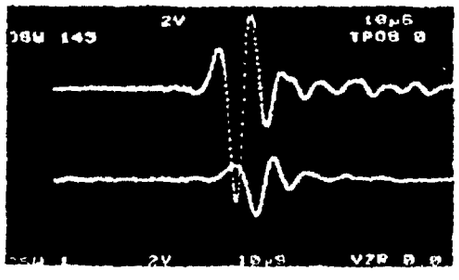

In Air

In Water

Fig. 38. Comparison of sand dollar skeleton wedge waves in air and in water.

CONCLUSIONS

A summary of the new findings was given at the beginning of the report. The results revealed gaps in fundamental physical understanding of littoral seismoacoustic phenomena in sandy sediments. It became evident that existing theories do not predict the measured waveforms in water-covered or drained sand. Further quantitative research is needed to characterize the complex seismoacoustic properties of various sand conditions (water-saturated, liquefied, drained, disturbed, compacted, etc...). Some of the questions that need to be answered include: What are the characteristics of different types of seismoacoustic waves existing in water-covered sand and partially-saturated sand? What are the effects of water content and air bubbles in sandy sediments on broadband pulsed compressional waves? What are the seismoacoustic properties of natural sand ripples compared to plowed ripples? What is the compressional wave velocity between 10 KHz and 70 KHz in sand near the beach? How does the frequency dependence of the compressional wave critical angle affect ambient noise and surfseism? How to determine grain to grain contact conditions and measure air bubbles content from broadband compressional wave data? How to use broadband compressional waves to monitor changes in sand grain to grain contact while coring? What are the effects of puddles near the beach on converting Rayleigh and Scholte waves? What are the effects of localized liquefied regions in shallow water along the seafloor on transmission loss? What is the combined dispersion effect of ripples, water level, and depth-dependence of velocities? Should the resonance frequency of bubbles in sediments decrease or increase compared to bubbles in water? Velea et al. [17] reported that for a 2.5 mm diameter bubble, the resonance frequency decreases from 1300 to 800 Hz in a natural sediment with a mean particle size of 30 μm, while it is mentioned in Reference [33] that in general, "the resonance frequency of the bubble in sediment is greater than for the equivalent bubble in water" due to the sediment shear modulus term. It is hoped that the outcome of this research would lead to future quantitative studies to gain fundamental understanding of acoustic oceanography and achieve reliable seismoacoustic detection of buried objects.

CONCLUSIONS

A summary of the new findings was given at the beginning of the report. The results revealed gaps in fundamental physical understanding of littoral seismoacoustic phenomena in sandy sediments. It became evident that existing theories do not predict the measured waveforms in water-covered or drained sand. Further quantitative research is needed to characterize the complex seismoacoustic properties of various sand conditions (water-saturated, liquefied, drained, disturbed, compacted, etc...). Some of the questions that need to be answered include: What are the characteristics of different types of seismoacoustic waves existing in water-covered sand and partially-saturated sand? What are the effects of water content and air bubbles in sandy sediments on broadband pulsed compressional waves? What are the seismoacoustic properties of natural sand ripples compared to plowed ripples? What is the compressional wave velocity between 10 KHz and 70 KHz in sand near the beach? How does the frequency dependence of the compressional wave critical angle affect ambient noise and surfseism? How to determine grain to grain contact conditions and measure air bubbles content from broadband compressional wave data? How to use broadband compressional waves to monitor changes in sand grain to grain contact while coring? What are the effects of puddles near the beach on converting Rayleigh and Scholte waves? What are the effects of localized liquefied regions in shallow water along the seafloor on transmission loss? What is the combined dispersion effect of ripples, water level, and depth-dependence of velocities? Should the resonance frequency of bubbles in sediments decrease or increase compared to bubbles in water? Velea et al. [17] reported that for a 2.5 mm diameter bubble, the resonance frequency decreases from 1300 to 800 Hz in a natural sediment with a mean particle size of 30 μm, while it is mentioned in Reference [33] that in general, "the resonance frequency of the bubble in sediment is greater than for the equivalent bubble in water" due to the sediment shear modulus term. It is hoped that the outcome of this research would lead to future quantitative studies to gain fundamental understanding of acoustic oceanography and achieve reliable seismoacoustic detection of buried objects.

REFERENCES

1. F. A. Boyle and N. P. Chotiros, "Experimental detection of a slow acoustic wave in sediment at shallow grazing angles," J. Acoust. Soc. Am. 91, 2615-2619 (1992).
2. T. G. Muir, C. W. Horton, and L. A. Thompson, "The penetration of highly directional acoustic beams into sediments," J. Sound Vib. 64, 539-551 (1979).
3. F. Padilla, M. de Billy, and G. Quentin, "Theoretical and experimental studies of surface waves on solid-fluid interfaces when the value of the fluid sound velocity is located between the shear and the longitudinal ones in the solid," J. Acoust. Soc. Am. 106(2), 666-673 (1999).
4. J. H. Ansell, The roots of the Stoneley wave equation for liquid-solid interfaces," Pure Appl. Geophys. 94, 172-188 (1972).
5. J. R. Chamuel, "An explanation for the anomalous ultrasonic slow wave in underwater sand," IEEE Trans. Ultrasonics and Freq. Control, 45(6), 1441-1443 (1998).
6. A. Maguer, S. Fioravanti, and A. Lovik, "Below critical angle detection of buried objects, " Proc. Oceans 1997 MTS/IEEE Vol.1, 512-517 (1997).
7. N. P. Chotiros, " Biot model of sound propagation in water-saturated sand, "J. Acoust. Soc. Am. 97(1), 199-214 (1995).
8. R. D. Stoll, "Comments on Biot model of sound propagation in water-saturated sand," J. Acoust. Soc. Am. 103(5), 2723-2725 (1998).
9. J. R. Chamuel, "Effect of ripples and depth-dependent shear wave velocity on converted seismoacoustic waves in sandy seafloor," ONR DRI Acoustics Workshop, APL, University of Washington, Seattle, Nov.3-4, 1998.
10. E. Pouliquen, A. P. Lyons, N. G. Pace, "The Helmholtz-Kirchhoff approach to modeling penetration of acoustic waves into rough seabeds," J. Acoust. Soc. Am. 104(3), Pt. 2, 1762 (1998).
11. E. I. Thorsos, D. R. Jackson, J. E. Moe, and K. L. Williams, "Modeling of subcritical penetration into sediments due to interface roughness," in *High Frequency Acoustics in Shallow Water*, edited by N. G. Pace, E. Pouliquen, O. Bergem, and A. P. Lyons, SACLATCEN Conf. Proc. series CP-45, 1997.
12. J. R. Chamuel, "Studies on the conversion of near-grazing underwater ultrasonic waves in a sandy seafloor," J. Acoust. Soc. Am. 104(3), Pt. 2, 1762 (1998).
13. H. J. Simpson, B. H. Souston, L. S. Couchman, "Measurement and modeling of sound propagation into unconsolidated water-saturated porous media in a laboratory," J. Acoust. Soc. Am. 104(3), Pt. 2, 1787 (1998).
14. W. A. Kuperman and H. Schmidt, "Self-consistent perturbation approach to rough surface scattering in stratified elastic media," J. Acoust. Soc. Am. 86(4) 1511-1522 (1989).
15. J. R. Chamuel, *Ultrasonic Studies of Transient Seismo-Acoustic Waves in Bounded Solids and Liquid/Solid Interfaces*, Sonoquest Advanced Ultrasonics Research, Report No. JRC-34-91, November 1991 (NTIS Document Accession No. AD-A243441).
16. J. R. Chamuel, "Scholte wave dispersion by rippled liquid/solid interface topography," J. Acoust. Soc. Am. 103(5), Pt.2, paper 2pUW17, 2902 (1998) and

in Proceedings of the 16th International. Congress on Acoustics and the 135th Meeting of the Acoustical Society of America, 20-26 June 1998. ,1365-1366 (1998).

17. D. Velea, "The effect of moisture on the propagation of compressional and shear waves in Ottawa sand," Ph.D. Thesis, The University of Mississippi, May 1998.
18. H. M. Tavossi and B. R. Tittman, "Acoustic signal attenuation, velocity, and filtering by beach sand, with different water content," J. Acoust. Soc. Am. 105(2), 1385 (1999).
19. J. R. Chamuel and G. H. Brooke, "Transient Scholte Wave Transmission Along Rough Liquid- Solid Interfaces" J. Acoust. Soc. Am. 83(4), 1336-1344 (1988).
20. J. R. Chamuel, *Ultrasonic Studies of Liquid/Solid Seismoacoustic Wave Phenomena*, Sonoquest Adv. Ultrason. Res., Report No. JRC-36-94, 1994. (NTIS # AD-A289644).
21. J. R. Chamuel, "Laboratory Studies on Pulsed Leaky Rayleigh Wave Components in a Water Layer over a Solid Bottom," in *Shear Waves in Marine Sediments*, edited by J. M. Hovem, M. D.Richardson, and R. D. Stoll, Kluwer Academic Publishers pp. 59-66 (1991).
22. J. R. Chamuel, "Backscattering of Scholte waves and near-grazing underwater acoustic waves by a trench at a liquid/solid interface," IEEE Trans.UFFC 41(6), 883-885 (1994).
23. J. R. Chamuel, "An explanation for the anomalous ultrasonic slow wave in underwater sand," IEEE Trans. on Ultrasonics, Ferroelectrics, and Frequency Control., 45(6) 1441-1443 (1998).
24. J. R. Chamuel, "Newly observed seismoacoustic wave characteristics in disturbed water-covered sand," J. Acoust. Soc. Am. 106(4), Pt.2, Paper 2aAO4, 2132 (1999).
25. R. Bachrach and A. Nur, "High-resolution shallow-seismic experiments in sand, Parts I and II, Geophysics 63(4), 1225-1233, 1234-1240 (1998).
26. M. Jacoby, J. Dvorkin, and X. Liu, "Elasticity of partially saturated frozen sand," Geophysics 61(1), 288-293 (1996).
27. M. J. Buckingham, "Theory of acoustic attenuation, dispersion, and pulse propagation in unconsolidated granular materials including marine sediments," J. Acoust. Soc. Am. 102(5), Pt. 1, 2579-2596 (1997).
28. M. D. Richardson, E. Muzi, B. Miaschi, and F. Turgutcan, "Shear wave velocity gradients in near-surface marine sediment," in Shear Waves in Marine Sediments, edited by J. M. Hovem, M. D. Richardson, and R. D. Stoll, Klumer Academic Publishers, Netherlands, 295-304 (1991).
29. J. Mobley, J. N. Marsh, C. S. Hall, M. S. Hughes, G. H. Brandenburger, and J. G. Miller, "Broadband measurements of phase velocity in Albunex® suspensions," J. Acoust. Soc. Am. 103(4), 2145-2153 (1998).
30. D. Velea, C. Hickey, J. M. Sabatier, and A. Kolaini, "Oscillation of bubbles released from needles in natural and artificial sediments," J. Acoust. Soc. Am. 106(4), 2391 (1999).
31. C. J. Hickey and J. M. Sabatier, "Measurement of two types of dilatational waves in an air-filled unconsolidated sand," J. Acoust. Soc. Am. 102(1), 128-136 (1997).

32. E. Smith, P. S. Wilson, F. W. Bacon, J. F. Manning, J. A. Behrens, and T. G. Muir, "Measurement and localization of interface wave reflections from a buried target," J. Acoust. Soc. Am. 103(5), Pt.1, 2333-2343 (1998).
33. H. Medwin and C. S. Clay, *Fundamentals of Acoustical Oceanography*, Academic Press, 1998 page 344.
34. E. A. Ash, R. M. De La Rue, and R. F. Humphryes, "Microsound Surface Waveguides," IEEE Trans. Microwave Theory and Tech., MTT-17, No. 11, 882-892 (1969).
35. P. E. Lagasse, "Analysis of a Dispersionfree Guide for Elastic Waves," Electronics Letters, 8(15), 372-373 (1972).
36. A. A. Maradudin, R. F. Wallis, D. L. Millis, and R. L. Ballard, "Vibrational Edge Modes in Finite Crystals," Physical Review B, 6(4), 1106-1111 (1972).
37. J. R. Chamuel, "Edge Waves along Immersed Elastic Elliptical Wedge with Range Dependent Apex Angle," IEEE 1993 Ultrasonics Symposium Proceedings, 313-318 (1993).
38. J. R. Chamuel, "Experimental observations on liquid/solid interface waves," J. Acoust. Soc. Am. Suppl. 1, Vol. 72, S99, (1982).

Proc. 16th Int. Congress Acoust. & 135th Meeting Acoust. Soc. Am., Seattle, June 1998

Scholte Wave Dispersion by Rippled Liquid/Solid Interface Topography

Jacques R. Chamuel

Sonoquest Advanced Ultrasonics Research, P. O. Box 81153, Wellesley Hills, MA 02181-0001

Abstract: Quantitative experimental results are presented characterizing the dispersion of Scholte waves propagating along a rippled surface of an immersed "soft" solid half-space. One model has a sinusoidal profile with a ratio of corrugation amplitude to wavelength of 0.25. Scholte and Rayleigh wave experimental dispersion results are compared with numerical results on Rayleigh wave dispersion along a "hard" corrugated solid half-space [N.E. Glass, R. Loudon, and A. A. Maradudin, Physical Review B 24, 6843-6861 (1981)]. The findings reveal that a rippled "soft" liquid/solid interface can decrease the velocity of high-frequency Scholte wave components propagating normal to the ripples by more than 70%.

INTRODUCTION

The effect of a rippled liquid/solid interface on the dispersion of Scholte waves is not known. Frequency-dependent multiple scattering phenomena occur as near-grazing underwater acoustic waves and Scholte waves interact with periodic seafloor topography having dimensions comparable to the wavelength. In order to develop physical understanding of the interaction of broadband transient underwater acoustic waves and Scholte waves with a rippled ocean bottom, experimental ultrasonic experiments were conducted on immersed isotropic "soft" models with a sinusoidally corrugated surface. Quantitative experimental results were obtained characterizing the dispersion of Rayleigh and Scholte waves caused by a periodic liquid/solid interface.

MODEL EXPERIMENTS AND RESULTS

A sinuoidal pattern was machined along the edge of a 4.5 mm thick Plexiglas plate. The spatial wavelength of the periodic pattern was 2 cm and the peak-to-peak amplitude was 1 cm. The measured Plexiglas velocities were as follows: compressional plate velocity = 2313 m/s, shear wave velocity = 1344 m/s, flat edge Rayleigh wave velocity = 1220 m/s, flat edge Scholte wave velocity = 1109 m/s. The top trace of Figure 1(a) compares the dispersed waveforms of Rayleigh and Scholte waves propagating along the periodic surface. Rayleigh and Scholte waves were obtained from air/Plexiglas and water/Plexiglas models, respectively. The Scholte waveform was stretched more to the right than the Rayleigh wave indicating that it was slower than the Rayleigh wave. The bottom trace of Figure 1(a) shows the arrival time of the corresponding Rayleigh wave along a flat surface (no

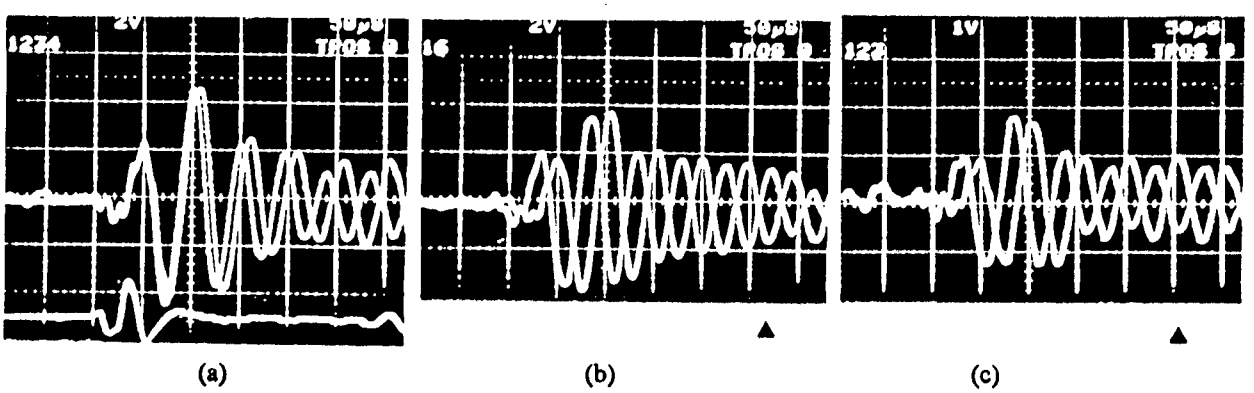

(a) (b) (c)

FIGURE 1. Comparison of received waveforms and arrival time; (a) Top Trace: Rayleigh and Scholte waves along corrugated surface (range x = 12 cm), Bottom Trace: reference Rayleigh wave from flat solid surface, (b) Rayleigh wave along corrugated surface detected at two positions separated by one corrugation cycle (2 cm), (c) Scholte wave along corrugated surface detected at the same two positions in (b).

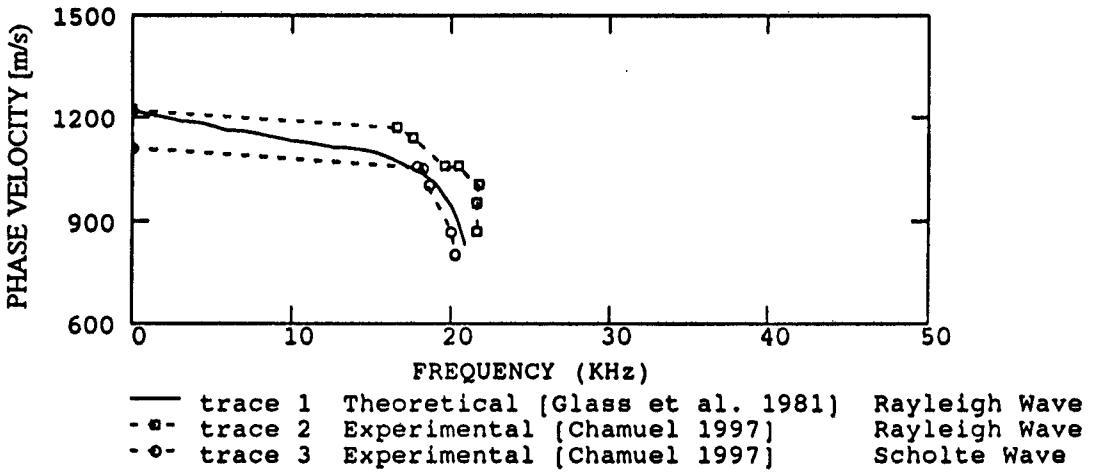

FIGURE 2. Rayleigh and Scholte wave dispersion experimental results compared with approximately scaled theoretical dispersion results by Glass et al. [1] on Rayleigh wave.

corrugation). Rayleigh and Scholte waves propagating along an isotropic elastic half-space are nondispersive. The source/receiver range was fixed at x = 12 cm. The vertical amplitude scale was arbitrary. Figure 1(b) compares the Rayleigh wave detected at two different locations separated by one cycle along the corrugation (x = 10 cm and x = 12 cm). The time delay between the two waveforms caused the corresponding Bragg frequency component to be shifted by 180° (arrow pointing to out of phase components). The measured Rayleigh wave Bragg frequency along this sinusoidal surface was 21.62 KHz. The periodic surface decreased the Rayleigh wave velocity from 1220 m/s to 865 m/s at the Bragg frequency. The corresponding Scholte wave experimental results, measured at the same two locations, are shown in Figure 1(c). The Scholte wave Bragg frequency was 20.2 KHz indicating that the Scholte wave velocity decreased from 1109 m/s to 808 m/s.

The Scholte and Rayleigh wave experimental dispersion results obtained from a "soft" elastic models are compared with replotted scaled numerical results [1] on Rayleigh wave dispersion for a "hard" corrugated solid half-space. The scaling was achieved by simply multiplying the dispersion curve by the Rayleigh wave velocity ratio between the theoretical "hard" model and the experimental "soft" model. This yields approximate results because Poisson's ratio was not changed. Figure 2 compares the Rayleigh and Scholte wave experimental dispersion results with scaled theoretical dispersion curve of Glass et al. The experimental results generally agreed with the Rayleigh wave theoretical results by Glass et al.. Work is in progress to compare the experimental results with Boström's calculated results [2] on Rayleigh waves. To the author's knowledge, there are no known published theoretical or numerical results characterizing the dispersion of Scholte waves by a large amplitude corrugated liquid/solid interface. Quantitative controlled laboratory ultrasonic measurements revealed that a rippled "soft" liquid/solid interface can decrease the velocity of high-frequency Scholte wave components propagating normal to the ripples by more than 70%. The findings indicate the potential importance of seafloor topography on acoustic inversion and detection of buried objects in shallow water.

ACKNOWLEDGEMENTS

Work supported by ONR.

REFERENCES

1. Glass, N. E., Loudon, R. and Maradudin, A. A., *Physical Review* B 24, 6843-6861 (1981).
2. Boström, A., *J. Acoust. Soc. Am.* 85 (4), 1549-1555 (1989).